NASA Technical Memorandum 4361

Pitot Survey of Exhaust Flow Field of a 2-D Scramjet Nozzle at Mach 6 With Air or Freon and Argon Used for Exhaust Simulation

William J. Monta

OCTOBER 1992

NASA

NASA Technical Memorandum 4361

Pitot Survey of Exhaust Flow Field of a 2-D Scramjet Nozzle at Mach 6 With Air or Freon and Argon Used for Exhaust Simulation

William J. Monta
Langley Research Center
Hampton, Virginia

National Aeronautics and Space Administration
Office of Management
Scientific and Technical Information Program
1992

Summary

A pitot-rake survey of the flow field in the simulated exhaust of a half-span scramjet nozzle model was conducted in the Langley 20-Inch Mach 6 Tunnel to provide additional data for computational fluid dynamics (CFD) code comparisons. A wind-tunnel model was tested with a 26-tube pitot rake that could be manually positioned along the mid-semispan plane of the model. The model nozzle configuration had an external expansion surface of 20° and an internal cowl expansion of 12°. Tests were also made using a flow fence (sidewall) to limit lateral expansion of the exhaust. Tests were conducted at a free-stream Reynolds number of approximately 6.5×10^6 per foot and a model angle of attack of −0.75°. Two exhaust gas mediums (air and a mixture of Freon 12 and argon) were tested at jet total pressures of about 28 and 14 psia.

This document presents the flow-field survey results in graphical as well as tabular form, and several observations concerning the results are discussed. The surveys reveal the major expected flow-field characteristics for each test configuration.

For a 50-percent Freon 12[1] and 50-percent argon mixture by volume (Fr-Ar), the exhaust jet pitot pressures were slightly higher than those for air. The addition of a flow fence slightly raised the pitot pressures for the Fr-Ar mixture, but it produced little change for air. For the Fr-Ar exhaust the plume was larger and the region between the shock wave and plume was smaller.

Introduction

The advent of the supersonic-combustion ramjet, or scramjet, engine opened the door to flight speeds well above Mach 6 for air-breathing propulsion systems. Because existing and proposed engine ground-test facilities could not provide data on engine performance in this flight regime, a flight research vehicle (X-24C) was proposed in the 1970's (refs. 1 and 2) to act as a scramjet test facility and to extend the aerodynamic flight data base beyond that obtained from the X-15 program. This new research vehicle program stimulated research at the Langley Research Center (ref. 3) as well as at other Government research facilities, but the cancellation of the program in the late 1970's resulted in a decline in research for air-breathing hypersonic facilities. Recently, interest in these types of aircraft has resurfaced as part of the National Aero-Space Plane Program or NASP (ref. 4), and although the technology requirements for this new program are vastly more challenging than those of the previous program, many of the basic issues affecting scramjet-powered aircraft are unchanged.

One of the most challenging issues concerning hypersonic, air-breathing aircraft is the efficient integration of the propulsion system with the airframe. Because of the large inlet-compression and nozzle-expansion ratios required for high Mach number flight, the entire undersurface of the airframe must be an integral part of the propulsion system. The lower rear portion of the airframe acts as part of the nozzle external expansion surface, and it can produce large force and moment contributions that significantly affect overall vehicle stability and trim; therefore, careful contouring of the external nozzle surfaces will be necessary to distribute these effects. Early analyses (refs. 5 and 6) to determine the severity of this problem within the Mach number range of 6 to 10 were limited to two-dimensional (2-D) solutions of flow in nozzles of arbitrary geometry, and impact theory aerodynamic programs were used to calculate aircraft longitudinal stability. This effort identified several nozzle geometries that had minimal effects on trim drag of a typical hypersonic configuration and generally established the effect of individual nozzle geometric parameters on forces and moments produced by the nozzle flow.

An experimental data base was established to confirm trends of the 2-D analyses and to provide data for a three-dimensional (3-D) flow field. Wind-tunnel tests for a 3-D three-module scramjet engine nozzle and a vehicle afterbody were conducted in the Langley 20-Inch Mach 6 Tunnel in the mid-1970's with air used to simulate the scramjet exhaust. The 3-D data (which are unpublished) provided forces and moments produced by different portions of the nozzle and by the nozzle as a whole. A method (ref. 7) was developed to simulate the scramjet exhaust flow using a Fr-Ar mixture and requiring the duplication of Mach number, nozzle static-pressure ratio, and ratio of specific heats at the engine combustor exit station. This technique was validated in a detonation tube for flight values of Reynolds number and enthalpy at Mach 6 and 8 (refs. 8 and 9) by comparing surface pressures on an external nozzle obtained for hydrogen-air combustion and for Fr-Ar mixtures. Two-dimensionsal surface pressure tests were reported in reference 10, and they utilized the simulant-gas method just discussed. For the tests reported therein, Mach number, static pressure, and ratio of specific heats at the combustor exit were approximated for the X-24C scramjet

[1]Freon: Registered trade name of E. I. du Pont de Nemours & Co.

operating in cruise flight at Mach 6 at dynamic pressures between 500 and 1000 lbf/ft^2. These conditions are considerably lower than those of the accelerating, high-dynamic-pressure flight proposed for NASP at Mach 6; consequently, engine combustor exit pressures for NASP would be greater than those originally contemplated for the experimental results reported in reference 10. For the tests, static pressure at the combustor exit was varied over a limited range for all the nozzle configurations, but in all cases, the exhaust flow was underexpanded (i.e., higher than the free-stream pressure) at the cowl lip (station 4). To provide additional data for CFD code comparisons, the present study was undertaken to survey the exhaust flow field of the same model.

The configuration chosen for these tests had an external expansion surface (ramp) of 20° and an internal cowl expansion of 12°. A 26-tube pitot rake, which spanned 5.0 in., was fabricated with a manually adjustable sting to permit locating the rake behind the cowl at distances of 0 to 6.36 in. The rake could be placed either vertically in the mid-semispan plane or horizontally so that 3-D spanwise surveys could be obtained; however, a lack of sufficient test time prevented testing with the rake in the latter orientation.

The investigation was conducted in the Langley 20-Inch Mach 6 Tunnel at a free-stream Reynolds number of 6.5×10^6 per foot and tunnel stagnation conditions of 365 psia (±5 psia) and 425°F (±10°F). The angle of attack was −0.75°, and configurations were tested with the flow fence on and off. An enhanced control system for the gas delivery apparatus was installed to be able to conduct successive runs that were reproducible to within ±1 psi of the same jet total pressure. Two simulant-gas mixtures, Fr-Ar and air, were used. Both mixtures were tested at 28 and 14 psia jet total pressures. Results are presented herein in graphical and tabular form with limited discussion. Results for one test condition have been published and compared with CFD solutions in reference 11.

Symbols

All data presented are based on measurements made in U.S. Customary units.

H	distance of rake pitot centerline to model surface, measured in rake tip plane, in.
h	combustor exit height, in.
M	Mach number
p	static pressure, psia
p_t	total pressure, psia
q	dynamic pressure, psia
T_t	stagnation temperature, °F
X, Y	axial and vertical coordinates of internal nozzle, in.
x	distance along instrumented nozzle surface from station 3, in.
α	angle of attack of model (fig. 2(a)), deg
β	angle between model reference line and external nozzle surface (fig. 2(b)), deg
γ	ratio of specific heats
ε	angle between model reference line and internal cowl surface (fig. 2(b)), deg

Subscripts:

j	jet nozzle exhaust flow
2	pitot pressure behind normal shock, psia
3	station 3, combustor exit station (fig. 2)
∞	free-stream conditions

Apparatus and Methods

Wind Tunnel

The Langley 20-Inch Mach 6 tunnel is a blowdown facility that uses air as the test medium. This tunnel has a test section 20.0 in. high by 20.0 in. wide in which the free-stream flow is generated by a 2-D fixed-geometry nozzle. The tunnel flow can be discharged either to evacuated spheres or to an annular air ejector, or to both simultaneously. The tunnel air is supplied from a 600-psia bottle field and is heated by an electrical resistance heater. A standard range of operating conditions of the tunnel are stagnation pressures from 30 to 525 psia, stagnation temperatures from 350° to 558°F, and free-stream unit Reynolds numbers from 0.7×10^6 to 9.0×10^6 per foot. Further details concerning the facility can be found in references 12 and 13.

Simulant-Gas System

For the present investigation, a simulant-gas mixture consisting of 50 percent argon and 50 percent Freon 12 by volume was used; air was also tested for comparison. The simulant-gas mixture was prepared and stored in a 22-ft^3 heated pressure vessel that contained approximately 220 lb of the mixture when filled to a pressure of 1500 psia at 500°F. Further details regarding the simulant-gas system are found in reference 10.

Model

The model for this investigation is the one that was utilized in the investigation of reference 10, and it represented a simplified version of the lower aft portion of a hypersonic research vehicle (X-24C) proposed in the 1970's (fig. 1). This figure also shows that the model has been installed in an inverted position. By using a half-span model of the vehicle afterbody, a larger model could be constructed. Detailed drawings of the model and rake are presented in figure 2. A three-view drawing of the test model is shown in figure 2(a). The geometry for the nozzle section of the model is shown in figure 2(b), in which the combustor exit station is denoted as station 3. The contour of the nozzle from the throat to station 3 was designed using the code of reference 14. For a combustor exit height of 0.60 in. and nozzle length of 1.08 in., the nozzle contour was calculated so that a Fr-Ar mixture would produce a Mach number M_3 of 1.7 at the combustor exit station (station 3). This same nozzle was also used for testing with air ($\gamma = 1.40$) as the simulant gas and resulted in an M_3 increase to 1.78 and a corresponding static pressure p_3 decrease relative to that for the Fr-Ar simulant gas at a given $p_{t,j}$ value.

Figure 2(c) details the pitot rake and rake support, and figure 3 shows a photograph of the assembled model with pitot rake. The model, which was mounted to a reflection plate that was strut supported from the tunnel floor, was fabricated from aluminum except for the plenum and internal nozzle, which were made from stainless steel. The model had a maximum length of 31.0 in., a height of 6.5 in., and width of 6.7 in. The model was set parallel to the tunnel floor, which had a slope of 0.75° to allow for boundary-layer growth, thus yielding a true model angle of attack of −0.75°. The 2-D effect of an expansion of this magnitude would be an increase in Mach number of 0.11 and a reduction of stream static pressure of 10.6 percent; both effects are considered negligible for these tests.

Instrumentation and Measurements

A flow-survey rake (fig. 2(c)) was constructed to measure the pitot-pressure distribution in the exhaust flow field of the external nozzle. The rake consisted of 26 pitot tubes; these tubes were equally spaced at 0.20 in. between centers and spanned a total of 5.0 in. A double wedge supported all the pitot tubes, which extended 0.50 in. from the wedge vertex. The rake was mounted on a shaft that was held parallel to the ramp surface by a bracket. The orientation of the rake to the nozzle and the coordinate system are shown in figure 2(d). This arrangement permitted the rake to be positioned at any station from $x = 2.14$ in. back to $x = 8.5$ in. This figure also shows the orientation of the rake to the nozzle and the coordinate system. Set screws were used to lock the shaft in position in the bracket. The rake was positioned to place the centerline of the bottom pitot tube 0.20 in. above the expansion surface. To reduce the magnitude of the maximum flow angle relative to any probe, the rake was inclined at an angle of 10° to the nozzle as shown in the figure. This inclination produced probe flow angles of approximately −10° near the ramp, 10° in the free stream, and up to 15° or 16° (at the highest jet pressures) near the edge of the plume at the first few survey stations aft of the cowl. Reference 15 indicates that a maximum error of approximately 1 percent reduction exists in pitot pressure because of a flow incidence of 10°.

Two orifices (p_3) were located within the nozzle on the cowl surface at the combustor-exit station (station 3). The model plenum was instrumented with a thermocouple ($T_{t,j}$) and a pitot tube ($p_{t,j}$) to measure stagnation conditions of the jet exhaust flow.

The rake pressures were measured with a 48-port module of electronically scanned pressure transducers that had a range of 0 to 15 psia with an accuracy of 0.25 percent of the full-scale range. The tunnel stagnation pressure was measured with a 1000-psia strain-gauge pressure transducer that had an accuracy of ±0.5 percent of the full-scale range.

In this wind tunnel, aerodynamic heating causes the stainless-steel nozzle blocks to expand slightly during the course of a test blow, which causes increases in the expansion ratio and Mach number. To account for these increases, a pitot probe was usually injected into the free stream from the ceiling of the test section at the beginning and end of each run (every $p_{t,j}$) to provide a calibration of the Mach number, which tends to vary with tunnel wall temperature. The Mach number for each data point was interpolated linearly with respect to time from the values calculated for the start-of-run and end-of-run probe Mach number results, where available. If only a single probe Mach number point was available, that value was used for all data points in the run. The pressure from the Mach probe was measured on a capacitance-type pressure transducer that provided an accuracy of approximately 0.5 percent of the measured pressure values. The indicated Mach number during a typical run could rise by 0.03 to 0.05 if the tunnel walls were initially at room temperature. This Mach number variation would lower the

dynamic pressure by as much as 3.5 percent and the static and pitot pressures by as much as 5.3 percent.

Gas chromatograph measurements of gas samples from each tank of the Fr-Ar mixture were made, and the content of mixtures was estimated to be 50 percent (±5 percent) Freon 12 by volume, thus resulting in a calculated ratio of specific heats γ of 1.22 (±0.015). This value of specific-heat ratio is representative of a hydrogen-air combustion process for a scramjet at $M = 6$.

Tests

The investigation was conducted in the Langley 20-Inch Mach 6 Tunnel at a free-stream Reynolds number of 6.5×10^6 per foot. Tunnel stagnation conditions for the test were 365 psia (±5 psia) and 425°F (±10°F). The dew point temperature of the tunnel airstream was maintained below −40°F, measured at atmospheric pressure, and usually ranged from −60°F to −70°F. An outline of the test program is presented in table I. Each configuration was tested with the rake positioned on the mid-semispan plane at a maximum of 11 different stations along the length of the external expansion-surface nozzle (x = 2.14, 2.50, 3.00, 3.50, 4.00, 4.50, 5.00, 5.50, 6.50, 7.50, and 8.50; see fig. 2(d)). The rake had to be repositioned manually between runs. Therefore, only one rake station could be obtained in a single run, although frequently the two test jet total pressures (28 and 14 psia) were obtained during a single run. An objective for these tests was to control the jet total pressures to within ±1 psi to facilitate the comparison of the experimental results with computational studies, and this objective generally was achieved.

Results and Discussion

Table I gives a summary of test conditions, and table II presents the flow-field survey results in tabular form for all test configurations. Figures 4 to 7 give these flow-field results in graphical form. These figures and tables show the pitot-pressure variation as a function of tube position. Figure 8 illustrates the major 2-D model flow-field characteristics. The major features of the flow-field survey measurements for all cases generally can be described as follows: The maximum pitot pressure occurs near the ramp at the first rake station, where the local Mach number is the lowest, and it decreases with increasing distance from the ramp as well as with increasing distance downstream from the cowl trailing edge as the jet flow expands over the external nozzle. A significant decrease in pressure values exists directly behind the cowl trailing edge for the first few stations because of the probes lying within the wake of the internal and external cowl boundary layers. The probes farthest away from the ramp lie in the nearly free-stream flow and register an almost constant pressure (approximately 10 psi) throughout a region down to the shock wave emanating from the cowl trailing edge. Inboard of this shock is a region of elevated pitot pressure which extends to the shear layer between the nozzle exhaust flow and the external flow. These elevated pressure levels primarily occur due to the reduced Mach number behind the shock. Little evidence exists of the cowl wake aft of the first several survey stations, and in this form of the results, there is no sign of the internal shock wave that should propagate from the cowl through the exhaust flow. The surveys seem to register the major expected flow-field characteristics for each test configuration.

For the Fr-Ar exhaust mixture, the pitot pressures were slightly higher than those for air, as would have been expected (fig. 9). The addition of a flow fence slightly raised the pitot pressures for the gas mixture, but it produced little change for air. Reduction of the jet total pressure produced proportionally lower values of the pitot pressures.

A noticeable difference exists between the results for air and those for Fr-Ar, particularly at the rearmost survey stations (fig. 9). For the Fr-Ar exhaust, the plume is larger and the region between the shock wave and plume is smaller.

Summary of Results

A pitot-rake survey of the flow field in the simulated exhaust of a half-span scramjet nozzle model was conducted in the Langley 20-Inch Mach 6 Tunnel. The nozzle configuration had an external expansion surface of 20° and an internal cowl expansion of 12°; a flow fence (sidewall) on the external nozzle surface also was tested. Tests were conducted at a free-stream Reynolds number of approximatley 6.5×10^6 per foot and a model angle of attack of −0.75°. The two exhaust gas mediums that were tested were air and a 50-percent Freon 12 and 50-percent argon mixture at jet total pressures of about 28 and 14 psia.

Flow-field survey results are presented in graphical as well as tabular form. Several observations concerning the results have been noted. The surveys seem to register the major expected flow-field characteristics for each test configuration. For the 50-percent Freon 12 and 50-percent argon exhaust mixture, the pitot pressures were slightly higher than those for air. The addition of a flow fence slightly raised the pitot pressures for the gas mixture, but it produced little change for air. For the

Freon 12-argon exhaust, the plume was larger and the region between the shock wave and plume was smaller.

NASA Langley Research Center
Hampton, VA 23681-0001
August 20, 1992

References

1. Hearth, Donald P.; and Preyss, Albert E.: Hypersonic Technology—Approach to an Expanded Program. *Astronaut. & Aeronaut.*, vol. 14, no. 12, Dec. 1976, pp. 20–37.

2. Towards Hypersonics. *Flight Int.*, vol. 108, no. 3477, Oct. 30, 1975, pp. 657–658.

3. Sabo, Frances E.; Cary, Aubrey M.; and Lawson, Shirley W.: *Compendium of NASA Langley Reports on Hypersonic Aerodynamics.* NASA TM-87760, 1987.

4. Colladay, Raymond S.: Rekindled Vision of Hypersonic Travel. *Aerosp. America,* vol. 25, no. 8, Aug. 1987, pp. 30–31, 34.

5. Johnston, P. J.; Cubbage, J. M.; and Weidner, J. P.: Studies of Engine-Airframe Integration on Hypersonic Aircraft. AIAA Paper No. 70-542, May 1970.

6. Small, William J.; Weidner, John P.; and Johnston, P. J.: *Scramjet Nozzle Design and Analysis as Applied to a Highly Integrated Hypersonic Research Airplane.* NASA TN D-8334, 1976.

7. Oman, R. A.; Foreman, K. M.; Leng, J.; and Hopkins, H. B.: *Simulation of Hypersonic Scramjet Exhaust.* NASA CR-2494, 1975.

8. Hopkins, H. B.; Konopka, W.; and Leng, J.: *Validation of Scramjet Exhaust Simulation Technique.* NASA CR-2688, 1976.

9. Hopkins, H. B.; Konopka, W.; and Leng, J.: *Validation of Scramjet Exhaust Simulation Technique at Mach 6.* NASA CR-3003, 1979.

10. Cubbage, James M.; and Monta, William J.: *Parametric Experimental Investigation of a Scramjet Nozzle at Mach 6 With Freon and Argon or Air Used for Exhaust Simulation.* NASA TP-3048, 1991.

11. Tatum, Kenneth E.; Monta, William J.; Witte, David W.; and Walters, Robert W.: Analysis of Generic Scramjet External Nozzle Flowfields Employing Simulant Gases. AIAA-90-5242, Oct. 1990.

12. Sterrett, James R.; and Emery, James C.: *Extension of Boundary-Layer-Separation Criteria to a Mach Number of 6.5 by Utilizing Flat Plates With Forward-Facing Steps.* NASA TN D-618, 1960.

13. Keyes, J. Wayne: *Force Testing Manual for the Langley 20-Inch Mach 6 Tunnel.* NASA TM-74026, 1977.

14. Johnson, Charles B.; Boney, Lillian R.; Ellison, James C.; and Erickson, Wayne D.: *Real-Gas Effects on Hypersonic Nozzle Contours With a Method of Calculation.* NASA TN D-1622, 1963.

15. Pope, Alan; and Goin, Kennith L.: *High-Speed Wind Tunnel Testing.* John Wiley & Sons, Inc., c.1965.

Table I. Summary of Test Conditions

x	Gas: 50 percent Freon 12 and 50 percent argon by volume											
	Flow fence on						Flow fence off					
	Run	Point	$p_{t,j}$	Run	Point	$p_{t,j}$	Run	Point	$p_{t,j}$	Run	Point	$p_{t,j}$
2.14	48	622	27.54	49	635	13.41	54	691	27.52	54	694	13.39
2.50	45	590	27.37	52	668	13.27	55	706	27.69	55	709	14.61
3.00	44	571	27.68	44	573	14.84	56	720	26.91	56	721	13.13
3.50	43	554	27.80	43	555	14.12	57	736	27.52	57	738	12.76
4.00				41	528	13.79	59	759	28.41	59	760	14.03
4.50	40	514	27.63	40	515	13.47	60	774	27.55	60	775	14.23
5.00							61	788	27.38	61	790	15.25
5.50	39	501	27.37	39	503	14.13	62	803	28.57	62	806	13.76
6.50	33	436	27.24	35	454	14.02	64	828	27.55	64	829	13.31
7.50	32	425	27.20	36	466	14.44	65	842	27.97	67	871	14.74
8.50	31	414	27.23	37	477	14.61	66	855	27.80	66	856	12.99

x	Gas: air											
	Flow fence on						Flow fence off					
	Run	Point	$p_{t,j}$	Run	Point	$p_{t,j}$	Run	Point	$p_{t,j}$	Run	Point	$p_{t,j}$
2.14	6	129	28.84	6	131	14.31	80	1009	27.73	80	1013	13.84
2.50	8	155	27.80	8	157	13.13						
3.00	9	170	27.51	9	173	13.97						
3.50	12	190	27.99	12	193	14.31	79	995	27.71	79	996	14.22
4.00	23	327	27.83	25	354	13.84						
4.50	26	366	27.51	26	368	13.96	77	982	27.60	77	983	14.01
5.00												
5.50	71	920	27.66	72	935	13.29	76	971	27.81	76	973	14.12
6.50	70	908	28.02	70	910	14.23						
7.50	69	896	27.96	69	898	14.52						
8.50	68	882	27.45	68	883	14.58						

Table II. Flow-Field Pitot Pressures

(a) Freon 12-argon mixture; fence on; $p_{t,j}$ of ≈28 psia

Point		622	590	571	554	514	501	436	425	414
M		6.00	6.02	6.00	5.99	6.00	6.00	6.02	6.02	6.01
$p_{t,\infty}$		360.0	361.2	359.8	360.8	360.3	359.0	359.1	361.3	361.2
$T_{t,\infty}$		433.8	419.5	425.0	419.0	430.6	426.7	413.7	430.5	421.0
$p_{t,j}$		27.54	27.37	27.68	27.80	27.63	27.37	27.24	27.20	27.23
$T_{t,j}$		452.6	481.0	478.7	470.2	443.1	460.4	441.4	450.0	456.3
q_∞		5.74	5.68	5.76	5.78	5.73	5.75	5.64	5.67	5.71
p_∞		0.23	0.22	0.23	0.23	0.23	0.23	0.22	0.22	0.23
p_3		6.88	7.75	7.87	7.48	7.90	7.38	7.42	7.37	7.16
x		2.14	2.50	3.00	3.50	4.50	5.50	6.50	7.50	8.50
Pitot no.	H	$p_{t,2}$	$p_{t,2}$	$p_{t,2}$	$p_{t,2}$	$p_{t,2}$	$p_{t,2}$	$p_{t,2}$	$p_{t,2}$	$p_{t,2}$
2	5.00	9.74	9.99	10.24	10.37	10.53	10.45	10.32	16.23	15.35
3	4.80	10.08	10.22	10.35	10.41	10.41	10.43	10.27	16.26	10.20
4	4.60	10.23	10.29	10.41	10.50	10.22	10.47	17.55	16.36	5.64
5	4.40	10.22	10.25	10.34	10.37	10.55	10.60	16.52	10.86	4.54
6	4.20	10.05	10.14	10.33	10.32	10.87	10.62	16.46	5.75	4.84
7	4.00	10.12	10.33	10.46	10.73	10.63	16.58	12.77	4.88	4.65
8	3.80	10.39	10.56	10.63	10.71	10.54	16.57	6.23	5.16	4.43
9	3.60	10.46	10.23	10.67	10.73	10.33	15.44	5.12	5.01	4.26
10	3.40	10.32	10.42	10.68	10.58	11.27	8.48	5.63	4.93	4.21
11	3.20	10.54	10.51	10.58	10.39	16.87	4.92	5.62	4.95	4.24
12	3.00	10.58	10.42	10.40	10.26	10.34	6.12	5.70	5.05	4.35
13	2.80	10.40	10.36	10.09	9.84	4.89	6.33	5.75	5.07	4.36
14	2.60	10.26	10.13	10.14	16.69	6.28	6.41	5.57	4.41	3.85
15	2.40	10.09	10.41	10.70	6.10	6.72	5.97	4.69	4.20	3.84
16	2.20	10.46	10.15	7.00	5.73	5.95	5.26	5.01	4.36	3.94
17	2.00	9.97	8.06	6.00	5.38	5.96	5.73	5.21	4.50	3.99
18	1.80	6.05	3.33	4.77	5.16	6.79	5.98	5.32	4.58	4.03
19	1.60	1.32	6.92	6.48	6.65	7.18	6.14	5.31	4.59	4.02
20	1.40	7.60	7.61	7.15	7.39	7.46	6.24	5.38	4.60	4.02
21	1.20	7.86	7.86	8.31	7.92	7.60	6.26	5.39	4.55	3.99
22	1.00	8.07	8.50	9.15	8.47	7.77	6.25	5.41	4.51	3.96
23	0.80	9.12	10.44	10.18	9.11	7.94	6.21	5.37	4.47	3.94
24	0.60	11.75	12.43	11.38	9.89	8.15	6.18	5.32	4.44	3.88
25	0.40	13.79	14.17	12.38	10.50	8.26	6.15	5.14	4.30	3.73
26	0.20	14.86	15.30	13.12	10.85	8.24	5.93	4.80	3.99	3.41

Table II. Continued

(a) $p_{t,j}$ of ≈14 psia

Point		635	668	573	555	528	515	503	454	466	477
M		6.03	6.01	6.01	6.00	6.02	6.01	6.01	6.01	6.01	6.01
$p_{t,\infty}$		360.5	361.1	361.4	360.1	362.5	361.2	360.4	359.4	360.2	360.8
$T_{t,\infty}$		433.3	427.9	430.7	429.5	429.7	429.8	429.3	419.8	421.8	431.4
$p_{t,j}$		13.41	13.27	14.84	14.12	13.79	13.47	14.13	14.02	14.44	14.61
$T_{t,j}$		421.8	426.8	429.0	425.5	421.4	408.3	411.3	422.9	428.5	438.4
q_∞		5.65	5.72	5.73	5.73	5.73	5.71	5.71	5.68	5.71	5.72
p_∞		0.22	0.23	0.23	0.23	0.23	0.23	0.23	0.23	0.23	0.23
p_3		3.61	3.20	3.59	2.92	3.33	3.23	3.41	3.05	3.51	3.58
x		2.14	2.50	3.00	3.50	4.00	4.50	5.50	6.50	7.50	8.50
Pitot no.	H	$p_{t,2}$	$p_{t,2}$	$p_{t,2}$	$p_{t,2}$	$p_{t,2}$	$p_{t,2}$	$p_{t,2}$	$p_{t,2}$	$p_{t,2}$	$p_{t,2}$
2	5.00	9.71	10.03	10.21	10.29	10.55	10.51	10.39	10.40	10.95	13.87
3	4.80	10.05	10.30	10.30	10.33	10.59	10.38	10.41	10.36	14.08	13.23
4	4.60	10.18	10.33	10.34	10.39	10.38	10.21	10.49	10.72	13.20	11.14
5	4.40	10.17	10.30	10.25	10.27	10.11	10.53	10.64	10.96	13.58	6.18
6	4.20	9.98	10.16	10.30	10.26	10.63	10.85	10.66	13.44	12.07	3.25
7	4.00	10.08	10.41	10.44	10.69	10.74	10.60	10.57	12.22	6.40	2.67
8	3.80	10.34	10.63	10.55	10.61	10.68	10.54	11.28	12.08	3.18	2.76
9	3.60	10.32	10.34	10.62	10.67	10.62	10.34	13.80	7.83	2.90	2.68
10	3.40	10.09	10.52	10.64	10.51	10.37	10.22	12.01	3.39	2.92	2.54
11	3.20	10.37	10.57	10.54	10.32	10.58	11.14	7.15	2.73	2.80	2.42
12	3.00	10.40	10.50	10.37	10.19	10.26	13.24	3.17	2.87	2.73	2.37
13	2.80	10.27	10.42	10.09	9.76	14.86	7.42	3.37	2.78	2.63	2.31
14	2.60	10.16	10.14	9.98	10.45	7.59	2.83	3.51	2.77	2.62	2.31
15	2.40	10.04	10.61	10.09	8.67	2.73	3.23	3.51	2.76	2.62	2.31
16	2.20	10.45	10.30	8.65	2.51	3.23	3.44	3.46	2.72	2.57	2.30
17	2.00	9.82	7.35	2.55	2.87	3.36	3.38	3.06	2.52	2.28	2.12
18	1.80	5.56	2.31	3.33	2.76	2.96	2.87	2.86	2.26	2.20	1.99
19	1.60	0.99	2.95	3.04	2.64	3.13	3.02	2.92	2.21	2.16	1.94
20	1.40	4.06	3.20	3.37	2.96	3.37	3.16	2.97	2.28	2.21	1.98
21	1.20	4.20	3.33	3.86	3.22	3.52	3.22	2.97	2.26	2.17	1.95
22	1.00	4.33	3.69	4.31	3.45	3.69	3.30	2.97	2.26	2.16	1.95
23	0.80	4.91	4.44	4.82	3.70	3.83	3.37	2.95	2.23	2.13	1.93
24	0.60	6.27	5.25	5.36	3.98	4.02	3.46	2.95	2.24	2.14	1.94
25	0.40	7.33	5.93	5.80	4.21	4.12	3.49	2.92	2.15	2.05	1.85
26	0.20	7.93	6.36	6.12	4.34	4.17	3.47	2.81	2.02	1.91	1.69

Table II. Continued

(b) Freon 12-argon mixture; fence off; $p_{t,j}$ of ≈28 psia

Point	691	706	720	736	759	774	788	803	828	842	855
M	6.00	6.01	6.01	6.01	5.99	5.99	5.99	6.00	6.00	6.00	6.005
$p_{t,\infty}$	359.7	361.3	360.4	361.5	361.0	360.6	361.4	361.0	361.5	361.9	359.8
$T_{t,\infty}$	426.5	415.2	421.7	421.5	429.0	431.2	428.0	425.5	428.7	419.2	431.5
$p_{t,j}$	27.52	27.69	26.91	27.52	28.41	27.55	27.38	28.57	27.55	27.97	27.796
$T_{t,j}$	444.3	437.8	430.0	432.1	452.7	479.8	470.6	450.1	271.8	280.0	283.4
q_∞	5.73	5.74	5.71	5.73	5.80	5.81	5.80	5.77	5.78	5.77	5.723
p_∞	0.23	0.23	0.23	0.23	0.23	0.23	0.23	0.23	0.23	0.23	0.227
p_3	6.48	6.66	6.52	6.85	6.68	6.63	6.63	7.01	6.59	6.74	6.752
x	2.14	2.50	3.00	3.50	4.00	4.50	5.00	5.50	6.50	7.50	8.5

Pitot no.	H	$p_{t,2}$	$p_{t,2}$	$p_{t,2}$	$p_{t,2}$	$p_{t,2}$	$p_{t,2}$	$p_{t,2}$	$p_{t,2}$	$p_{t,2}$	$p_{t,2}$	$p_{t,2}$
2	5.00	9.76	10.02	10.20	10.35	10.56	10.59	10.44	10.52	10.49	16.18	15.126
3	4.80	10.06	10.27	10.31	10.40	10.57	10.44	10.37	10.56	10.50	16.13	9.282
4	4.60	10.19	10.31	10.37	10.45	10.38	10.30	10.65	10.60	15.04	16.66	5.008
5	4.40	10.20	10.27	10.28	10.32	10.31	10.62	10.74	10.74	16.45	12.94	4.005
6	4.20	10.02	10.15	10.29	10.20	10.67	10.90	10.81	10.40	15.62	6.32	4.304
7	4.00	10.10	10.37	10.41	10.61	10.98	10.66	10.48	16.56	14.92	4.26	4.127
8	3.80	10.37	10.62	10.52	10.58	10.65	10.54	10.59	16.54	8.16	4.70	3.876
9	3.60	10.43	10.31	10.56	10.65	10.55	10.42	16.25	15.26	4.52	4.53	3.656
10	3.40	10.28	10.55	10.56	10.55	10.28	10.28	16.77	7.95	5.27	4.39	3.543
11	3.20	10.53	10.62	10.53	10.36	10.60	16.85	9.78	4.82	5.31	4.31	3.483
12	3.00	10.57	10.53	10.39	10.45	14.62	11.09	4.79	5.96	5.34	4.30	3.456
13	2.80	10.40	10.40	10.12	9.89	14.65	4.78	5.56	6.08	5.41	4.35	3.488
14	2.60	10.22	10.12	10.08	16.49	5.23	5.38	6.02	6.16	5.40	4.13	3.187
15	2.40	10.04	10.61	10.37	5.36	5.24	5.98	6.05	5.74	4.74	3.59	2.959
16	2.20	10.49	10.27	7.23	5.48	5.43	5.76	4.99	5.03	4.54	3.69	3.012
17	2.00	9.89	8.65	5.20	5.05	4.62	5.15	5.29	5.49	4.76	3.86	3.083
18	1.80	5.71	3.89	4.21	4.96	5.63	5.83	5.63	5.74	4.81	3.93	3.105
19	1.60	1.24	6.26	5.51	6.25	6.32	6.17	5.80	5.86	4.79	4.01	3.119
20	1.40	7.51	6.73	6.06	6.96	6.77	6.40	5.95	5.97	4.74	4.00	3.125
21	1.20	7.75	6.94	7.00	7.42	7.14	6.53	6.03	5.98	4.68	3.94	3.102
22	1.00	7.93	7.52	7.84	7.90	7.52	6.69	6.10	5.97	4.64	3.88	3.077
23	0.80	8.90	9.24	8.73	8.45	7.89	6.85	6.16	5.93	4.62	3.82	3.049
24	0.60	11.26	11.04	9.76	9.11	8.29	7.03	6.27	5.91	4.62	3.74	3.011
25	0.40	13.53	12.52	10.58	9.59	8.58	7.13	6.31	5.83	4.52	3.62	2.899
26	0.20	14.53	13.42	11.16	9.87	8.70	7.12	6.20	5.57	4.22	3.35	2.674

Table II. Continued

(b) $p_{t,j}$ of ≈14 psia

Point	694	709	721	738	760	775	790	806	829	871	856
M	6.02	6.02	6.02	6.02	6.00	6.00	6.00	6.01	6.01	6.01	6.011
$p_{t,\infty}$	361.9	361.6	361.1	359.3	361.5	361.6	362.0	360.8	362.3	362.3	361.5
$T_{t,\infty}$	421.9	431.0	425.5	428.9	428.8	432.9	433.5	425.3	425.6	425.5	421.2
$p_{t,j}$	13.39	14.61	13.13	12.76	14.03	14.23	15.25	13.76	13.31	14.74	12.987
$T_{t,j}$	395.8	402.4	405.1	413.5	412.6	446.0	439.8	418.9	273.5	287.1	289.1
q_∞	5.71	5.69	5.69	5.66	5.76	5.78	5.77	5.73	5.75	5.74	5.728
p_∞	0.23	0.22	0.22	0.22	0.23	0.23	0.23	0.23	0.23	0.23	0.227
p_3	3.09	3.45	2.93	2.93	3.23	3.70	3.91	3.89	3.33	3.51	2.74
x	2.14	2.50	3.00	3.50	4.00	4.50	5.00	5.50	6.50	7.50	8.5

Pitot no.	H	$p_{t,2}$	$p_{t,2}$	$p_{t,2}$	$p_{t,2}$	$p_{t,2}$	$p_{t,2}$	$p_{t,2}$	$p_{t,2}$	$p_{t,2}$	$p_{t,2}$	$p_{t,2}$
2	5.00	9.73	9.98	10.19	10.22	10.50	10.53	10.39	10.46	10.47	10.68	11.786
3	4.80	10.03	10.21	10.29	10.26	10.50	10.40	10.37	10.51	10.49	14.32	12.111
4	4.60	10.16	10.26	10.34	10.31	10.32	10.29	10.65	10.58	10.77	13.10	11.369
5	4.40	10.17	10.18	10.24	10.18	10.27	10.61	10.75	10.72	10.56	13.39	8.998
6	4.20	9.98	10.09	10.27	10.05	10.64	10.89	10.80	10.37	13.93	12.23	4.634
7	4.00	10.06	10.31	10.39	10.52	10.90	10.65	10.46		12.57	6.50	2.383
8	3.80	10.33	10.55	10.49	10.46	10.61	10.53	10.56	15.81	11.93	3.12	2.082
9	3.60	10.37	10.20	10.54	10.55	10.51	10.39	10.03	14.27	7.87	2.74	2.152
10	3.40	10.23	10.48	10.54	10.44	10.24	10.11	15.21	11.81	3.40	2.82	2.048
11	3.20	10.47	10.51	10.51	10.23	10.49	15.29	12.40	5.67	2.99	2.69	1.936
12	3.00	10.48	10.43	10.37	10.33	10.15	13.03	6.26	3.20	3.12	2.55	1.831
13	2.80	10.36	10.33	10.11	9.73	14.34	6.45	3.13	3.83	3.08	2.48	1.756
14	2.60	10.21	10.09	10.00	12.04	7.31	2.88	3.95	3.88	3.07	2.43	1.697
15	2.40	10.05	10.49	10.13	7.54	2.70	3.73	4.06	3.88	3.08	2.43	1.664
16	2.20	10.47	10.11	8.81	2.33	3.17	3.88	3.99	3.76	3.02	2.39	1.620
17	2.00	9.76	7.01	2.29	2.89	3.27	3.73	3.42	3.16	2.69	2.15	1.594
18	1.80	5.40	2.26	2.99	2.80	2.94	3.32	3.40	3.26	2.47	2.04	1.487
19	1.60	0.91	3.26	2.54	2.70	3.13	3.52	3.50	3.31	2.45	2.07	1.321
20	1.40	3.66	3.55	2.83	3.05	3.37	3.66	3.60	3.38	2.44	2.07	1.307
21	1.20	3.78	3.67	3.20	3.26	3.56	3.75	3.64	3.37	2.41	2.04	1.294
22	1.00	3.88	4.00	3.59	3.48	3.74	3.84	3.68	3.37	2.39	2.01	1.282
23	0.80	4.34	4.84	4.01	3.72	3.91	3.93	3.71	3.35	2.39	1.98	1.274
24	0.60	5.47	5.79	4.50	4.02	4.10	4.03	3.78	3.35	2.39	1.95	1.383
25	0.40	6.46	6.58	4.85	4.20	4.22	4.07	3.79	3.29	2.33	1.88	1.802
26	0.20	6.99	7.06	5.11	4.33	4.27	4.06	3.72	3.14	2.16	1.74	1.158

Table II. Continued

(c) Air; fence on; $p_{t,j}$ of ≈28 psia

Point		129	155	170	190	327	366	920	908	896	882
M		6.03	6.01	6.03	6.02	6.02	6.03	6.01	6.01	6.00	5.99
$p_{t,\infty}$		365.2	358.3	364.9	360.4	360.6	360.8	359.6	360.4	360.1	360.9
$T_{t,\infty}$		435.7	428.7	426.2	431.0	427.8	428.3	420.3	426.4	422.1	423.1
$p_{t,j}$		28.30	27.28	26.99	27.46	27.30	26.99	27.14	27.49	27.43	26.94
$T_{t,j}$		0.0	153.4	148.9	47.4	129.2	131.4	168.5	149.2	137.0	121.9
q_∞		5.71	5.69	5.73	5.66	5.68	5.65	5.72	5.73	5.76	5.79
p_∞		0.22	0.23	0.23	0.22	0.22	0.22	0.23	0.23	0.23	0.23
p_3		5.80	5.68	5.43	5.88	6.69	6.60	5.67	5.68	5.67	5.63
x		2.14	2.50	3.00	3.50	4.00	4.50	5.50	6.50	7.50	8.50
Pitot no.	H	$p_{t,2}$	$p_{t,2}$	$p_{t,2}$	$p_{t,2}$	$p_{t,2}$	$p_{t,2}$	$p_{t,2}$	$p_{t,2}$	$p_{t,2}$	$p_{t,2}$
2	5.00	9.71	9.64	9.95	10.21	10.28	10.45	10.30	10.46	16.01	12.66
3	4.80	9.97	9.87	10.03	10.31	10.35	10.31	10.40	10.58	14.89	11.50
4	4.60	10.08	9.91	10.07	10.32	10.20	9.96	10.57	10.87	13.43	10.78
5	4.40	10.06	9.83	10.01	10.16	9.91	10.21	10.74	16.44	12.09	7.16
6	4.20	9.94	9.75	9.99	10.11	10.32	10.55	10.47	14.88	10.00	4.43
7	4.00	10.00	9.97	10.18	10.49	10.61	10.63	10.66	13.34	6.23	4.59
8	3.80	10.24	10.20	10.19	10.39	10.42	10.46	16.49	10.33	4.36	4.68
9	3.60	10.30	9.89	10.18	10.51	10.37	10.33	14.68	5.65	4.99	4.53
10	3.40	10.06	10.13	10.22	10.43	10.21	10.20	10.88	4.03	5.17	4.46
11	3.20	10.31	10.15	10.27	10.32	10.41	16.87	5.39	5.21	5.18	4.41
12	3.00	10.23	10.13	10.17	10.19	10.20	12.67	4.15	5.96	5.22	4.38
13	2.80	10.28	10.03	9.96	9.80	15.47	5.76	5.04	6.18	5.28	4.39
14	2.60	10.13	9.81	10.01	16.54	6.20	5.30	5.56	6.17	5.22	4.17
15	2.40	10.09	10.18	10.05	7.26	5.59	5.77	5.80	5.41	4.31	3.67
16	2.20	10.43	9.95	8.91	5.20	5.88	5.20	4.79	4.92	4.26	3.77
17	2.00	9.89	7.33	4.47	5.44	4.40	4.80	5.25	5.03	4.26	3.85
18	1.80	5.73	2.93	4.36	4.69	5.15	5.86	5.47	5.15	4.20	3.85
19	1.60	1.37	6.20	5.29	5.08	5.94	6.43	5.60	5.16	4.25	3.79
20	1.40	7.49	6.57	5.41	5.48	7.06	6.91	5.71	5.20	4.30	3.74
21	1.20	7.77	6.65	5.65	6.53	7.69	7.30	5.79	5.17	4.30	3.73
22	1.00	7.89	6.88	6.42	7.52	8.29	7.72	5.91	5.15	4.26	3.71
23	0.80	8.78	7.91	8.12	8.40	8.89	8.13	6.03	5.12	4.20	3.71
24	0.60	10.51	10.40	9.60	9.27	9.55	8.51	6.14	5.12	4.14	3.67
25	0.40	13.00	12.58	10.86	10.00	10.07	8.75	6.15	5.00	4.05	3.55
26	0.20	14.52	13.73	11.67	10.51	10.32	8.72	5.97	4.67	3.75	3.18

Table II. Continued

(c) $p_{t,j}$ of ≈14 psia

Point	131	157	173	193	354	368	935	910	898	883
M	6.04	6.02	6.03	6.04	6.03	6.03	6.00	6.01	6.01	6.00
$p_{t,\infty}$	364.9	361.2	366.1	361.5	359.6	358.8	359.9	362.4	361.0	361.0
$T_{t,\infty}$	423.9	440.3	421.4	425.6	426.6	423.9	418.3	437.1	424.4	424.7
$p_{t,j}$	14.04	12.88	13.71	14.04	13.58	13.70	13.04	13.96	14.25	14.30
$T_{t,j}$	397.0	392.5	0.0	80.1	135.2	135.3	172.1	155.3	146.9	133.5
q_∞	5.66	5.68	5.71	5.63	5.63	5.59	5.74	5.74	5.73	5.76
p_∞	0.22	0.22	0.22	0.22	0.22	0.22	0.23	0.23	0.23	0.23
p_3	2.73	2.39	2.56	2.93	2.96	2.83	2.63	2.81	3.11	2.82
x	2.14	2.50	3.00	3.50	4.00	4.50	5.50	6.50	7.50	8.50

Pitot no.	H	$p_{t,2}$	$p_{t,2}$	$p_{t,2}$	$p_{t,2}$	$p_{t,2}$	$p_{t,2}$	$p_{t,2}$	$p_{t,2}$	$p_{t,2}$	$p_{t,2}$
2	5.00	9.61	9.65	9.94	10.17	10.32	10.35	10.40	10.46	10.42	11.54
3	4.80	9.92	9.88	10.02	10.25	10.41	10.19	10.45	10.57	13.65	10.53
4	4.60	10.02	9.93	10.06	10.27	10.19	9.83	10.63	10.87	12.38	9.39
5	4.40	9.98	9.85	9.99	10.12	9.88	10.10	10.79	10.33	11.17	8.70
6	4.20	9.84	9.76	9.97	10.07	10.28	10.45	10.53	13.33	10.00	8.01
7	4.00	9.91	9.98	10.16	10.42	10.52	10.50	10.70	11.90	8.45	4.27
8	3.80	10.16	10.21	10.09	10.31	10.43	10.35	10.57	10.54	5.73	2.66
9	3.60	10.21	9.84	10.14	10.46	10.42	10.22	12.82	8.41	3.20	2.83
10	3.40	9.93	10.11	10.18	10.40	10.25	10.10	11.14	4.92	3.04	2.79
11	3.20	10.19	10.13	10.24	10.28	10.47	10.18	8.12	2.79	3.27	2.67
12	3.00	10.12	10.13	10.15	10.18	10.20	12.41	4.17	2.94	3.22	2.57
13	2.80	10.15	10.05	9.95	9.80	13.36	8.00	2.33	3.43	3.21	2.53
14	2.60	10.04	9.84	10.00	10.39	8.26	3.29	2.90	3.53	3.20	2.51
15	2.40	10.01	10.21	10.03	8.45	3.16	2.77	3.25	3.55	3.19	2.52
16	2.20	10.34	9.96	9.14	2.77	3.31	3.06	3.36	3.50	3.08	2.53
17	2.00	9.79	7.04	2.46	3.48	3.21	3.03	3.27	2.98	2.51	2.30
18	1.80	5.62	2.56	3.27	3.11	2.58	2.61	2.59	2.65	2.38	2.01
19	1.60	1.05	2.74	2.58	2.63	2.75	2.84	2.64	2.63	2.42	1.97
20	1.40	3.64	2.88	2.63	2.86	3.22	3.11	2.72	2.64	2.44	1.95
21	1.20	3.80	2.93	2.77	3.30	3.53	3.28	2.75	2.62	2.43	1.94
22	1.00	3.86	3.04	3.17	3.83	3.85	3.46	2.80	2.61	2.40	1.93
23	0.80	4.30	3.53	3.93	4.30	4.14	3.63	2.86	2.60	2.37	1.93
24	0.60	5.18	4.53	4.70	4.77	4.45	3.80	2.93	2.61	2.34	1.89
25	0.40	6.30	5.51	5.38	5.14	4.67	3.88	2.93	2.53	2.28	1.82
26	0.20	7.05	6.10	5.82	5.38	4.77	3.86	2.80	2.32	2.09	1.61

Table II. Continued

(d) Air; fence off; $p_{t,j}$ of ≈28 psia

Point		1009	995	982	971
M		6.02	6.01	6.02	6.00
$p_{t,\infty}$		359.7	359.7	359.0	361.6
$T_{t,\infty}$		420.6	426.1	426.2	435.5
$p_{t,j}$		27.21	27.18	27.08	27.29
$T_{t,j}$		131.0	128.5	128.8	123.8
q_∞		5.68	5.70	5.66	5.76
p_∞		0.22	0.23	0.22	0.23
p_3		5.66	5.68	5.65	5.69
x		2.14	3.50	4.50	5.50
Pitot no.	H	$p_{t,2}$	$p_{t,2}$	$p_{t,2}$	$p_{t,2}$
2	5.00	9.79	10.36	10.44	10.47
3	4.80	10.15	10.43	10.27	10.47
4	4.60	10.31	10.40	10.10	10.61
5	4.40	10.30	10.33	10.36	10.78
6	4.20	10.10	10.26	10.65	10.53
7	4.00	10.25	10.58	10.54	10.74
8	3.80	10.57	10.68	10.46	16.55
9	3.60	10.53	10.62	10.37	14.79
10	3.40	10.29	10.55	10.14	11.20
11	3.20	10.41	10.43	16.66	5.53
12	3.00	10.42	10.54	12.76	4.11
13	2.80	10.33	9.89	5.76	5.04
14	2.60	10.30	16.71	4.67	5.59
15	2.40	10.23	6.72	5.25	5.85
16	2.20	10.73	5.45	4.83	4.83
17	2.00	10.13	5.39	4.14	5.21
18	1.80	5.79	4.72	5.12	5.42
19	1.60	1.55	5.05	5.73	5.56
20	1.40	7.74	5.48	6.24	5.67
21	1.20	7.93	6.43	6.60	5.75
22	1.00	8.06	7.47	6.93	5.86
23	0.80	8.86	8.34	7.22	5.99
24	0.60	10.64	9.19	7.51	6.13
25	0.40	12.94	9.89	7.69	6.21
26	0.20	14.60	10.36	7.71	6.06

Table II. Concluded

(d) Air; fence off; $p_{t,j}$ of ≈14 psia

Point		1013	996	983	973
M		6.03	6.02	6.03	6.02
$p_{t,\infty}$		360.6	359.0	360.6	362.0
$T_{t,\infty}$		424.2	427.5	426.7	429.9
$p_{t,j}$		13.58	13.95	13.74	13.85
$T_{t,j}$		133.4	131.2	130.9	127.7
q_∞		5.65	5.66	5.66	5.71
p_∞		0.22	0.22	0.22	0.23
p_3		2.76	2.87	2.75	2.85
x		2.14	3.50	4.50	5.50
Pitot no.	H	$p_{t,2}$	$p_{t,2}$	$p_{t,2}$	$p_{t,2}$
2	5.00	9.76	10.31	10.45	10.30
3	4.80	10.11	10.35	10.24	10.40
4	4.60	10.26	10.30	10.08	10.56
5	4.40	10.24	10.26	10.36	10.72
6	4.20	10.04	10.18	10.66	10.40
7	4.00	10.19	10.50	10.52	10.62
8	3.80	10.50	10.59	10.46	10.45
9	3.60	10.46	10.53	10.36	12.96
10	3.40	10.18	10.48	10.12	11.23
11	3.20	10.32	10.34	10.35	7.76
12	3.00	10.34	10.46	12.37	3.91
13	2.80	10.25	9.83	7.84	2.43
14	2.60	10.23	10.85	3.21	3.12
15	2.40	10.17	8.16	2.77	3.45
16	2.20	10.65	2.72	3.03	3.57
17	2.00	10.04	3.49	2.99	3.38
18	1.80	5.71	3.09	2.59	2.81
19	1.60	0.93	2.63	2.84	2.87
20	1.40	3.87	2.88	3.12	2.95
21	1.20	3.96	3.30	3.30	2.99
22	1.00	4.02	3.82	3.46	3.04
23	0.80	4.41	4.29	3.60	3.10
24	0.60	5.33	4.77	3.76	3.17
25	0.40	6.39	5.12	3.83	3.19
26	0.20	7.13	5.36	3.83	3.06

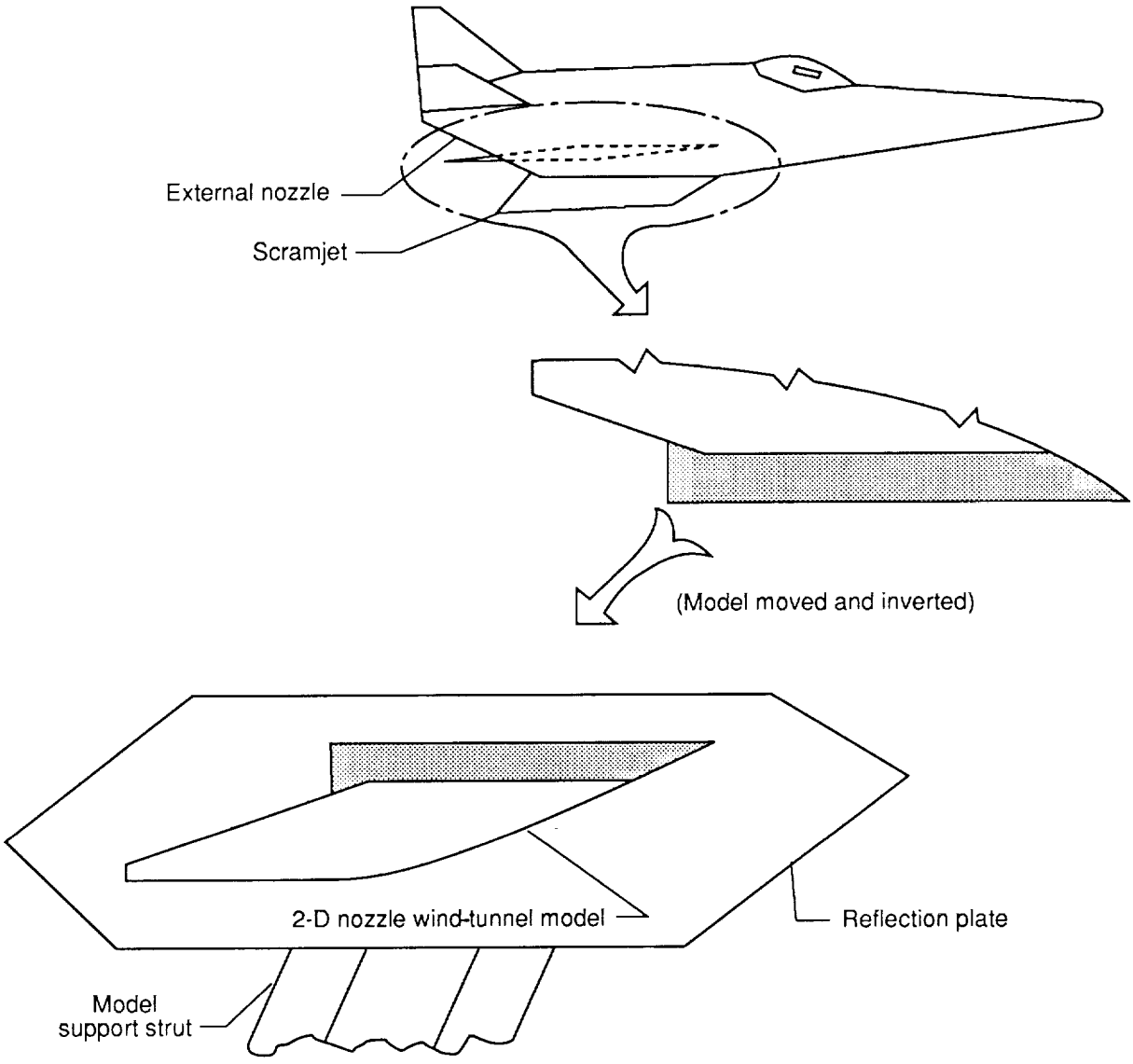

Figure 1. Genesis of wind-tunnel model.

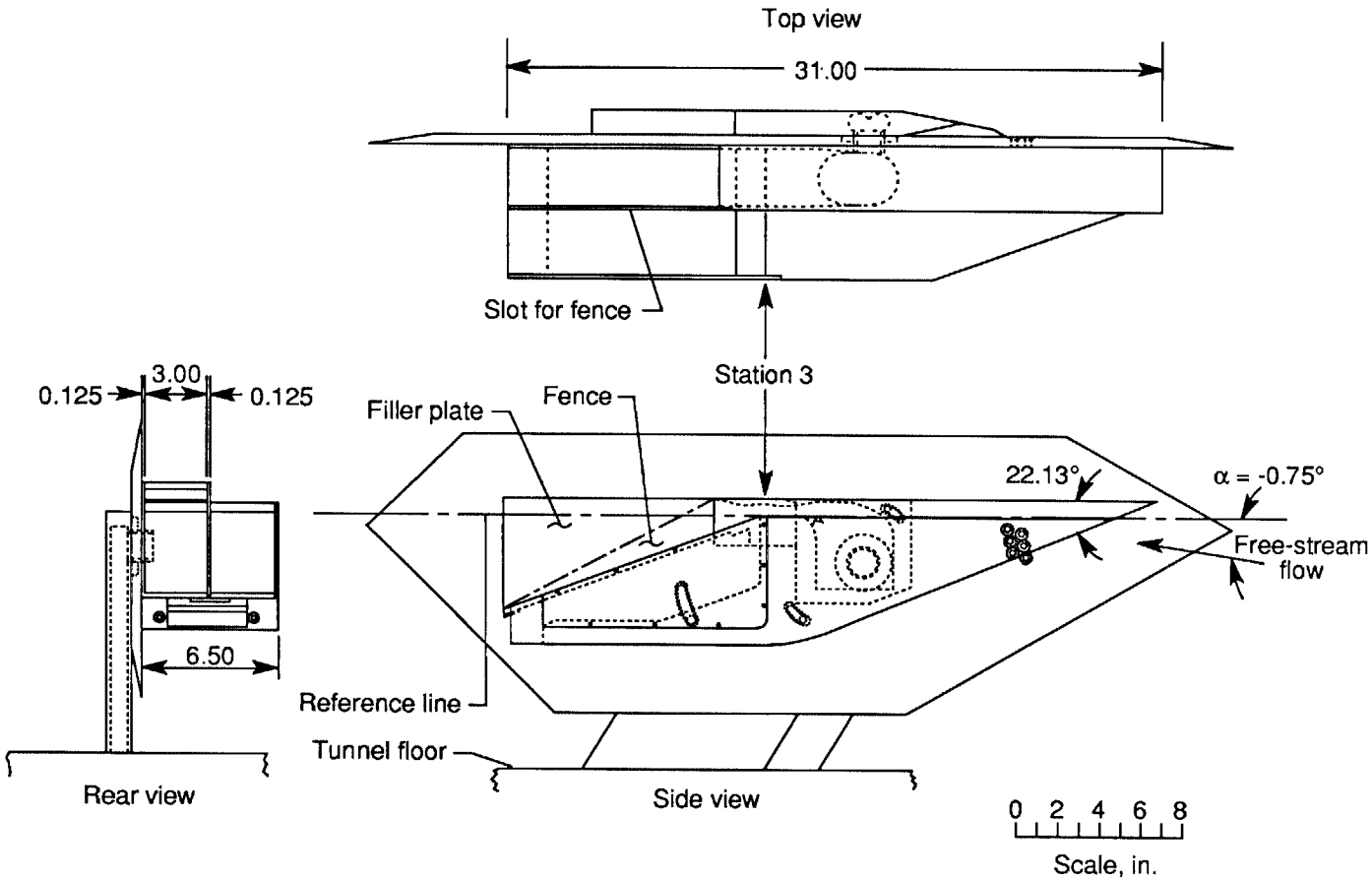

(a) Three-view drawing of model.

Figure 2. Drawings of model and rake. All linear dimensions are in inches.

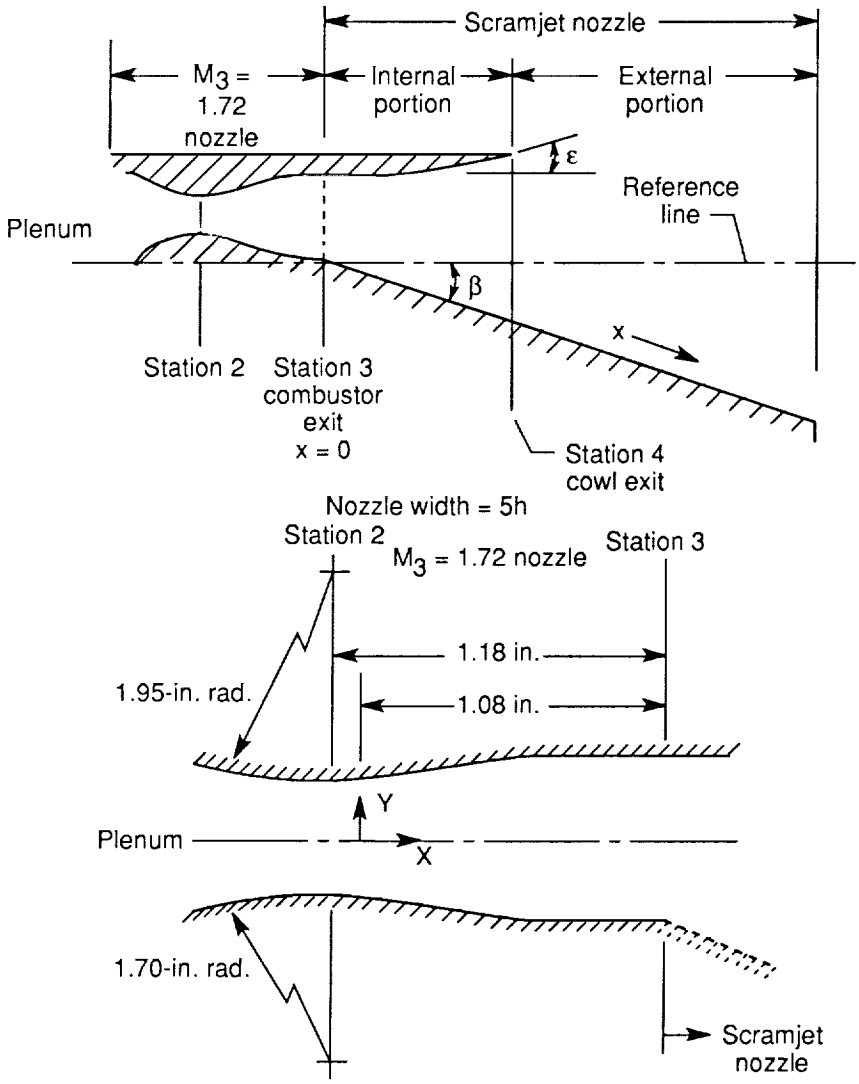

X	0	0.050	0.101	0.140	0.180	0.241	0.279	0.337	0.407	0.492	0.576	0.728	0.874	1.080
Y	0.212	0.216	0.221	0.226	0.232	0.242	0.248	0.256	0.266	0.275	0.283	0.293	0.298	0.300

(b) Nozzle details.

Figure 2. Continued.

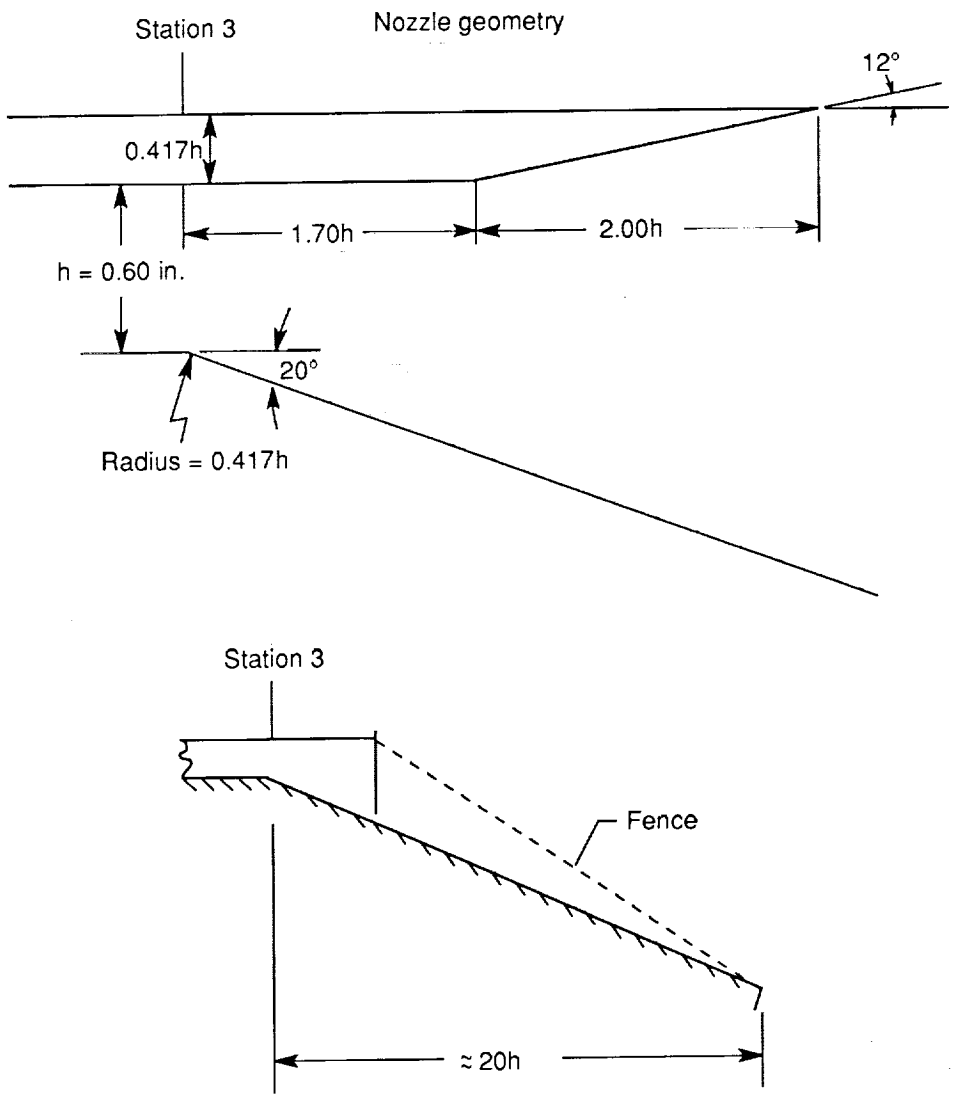

(b) Concluded.

Figure 2. Continued.

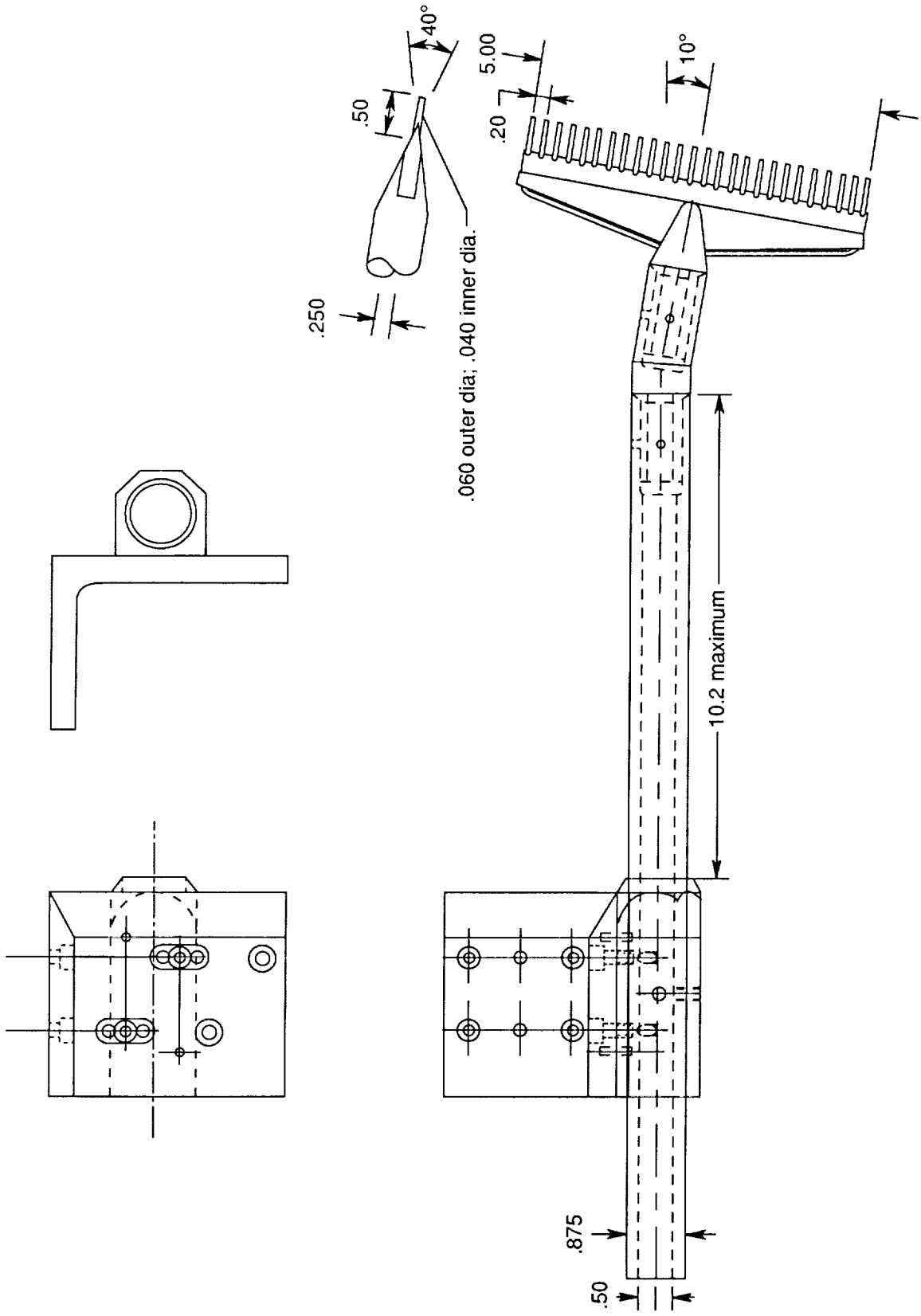

(c) Drawing of pitot rake and support.

Figure 2. Continued.

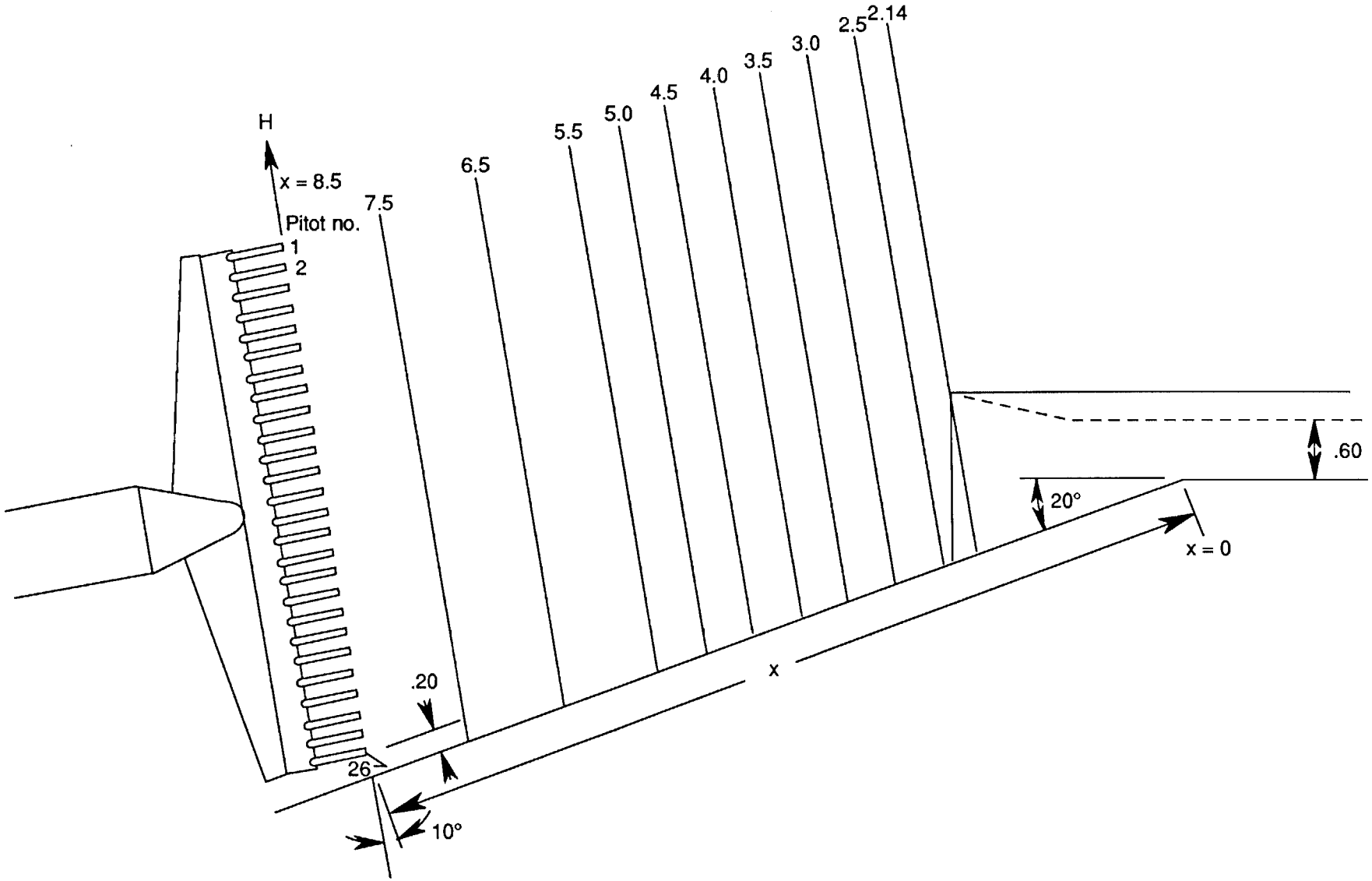

(d) Sketch of rake positions and coordinate system.

Figure 2. Concluded.

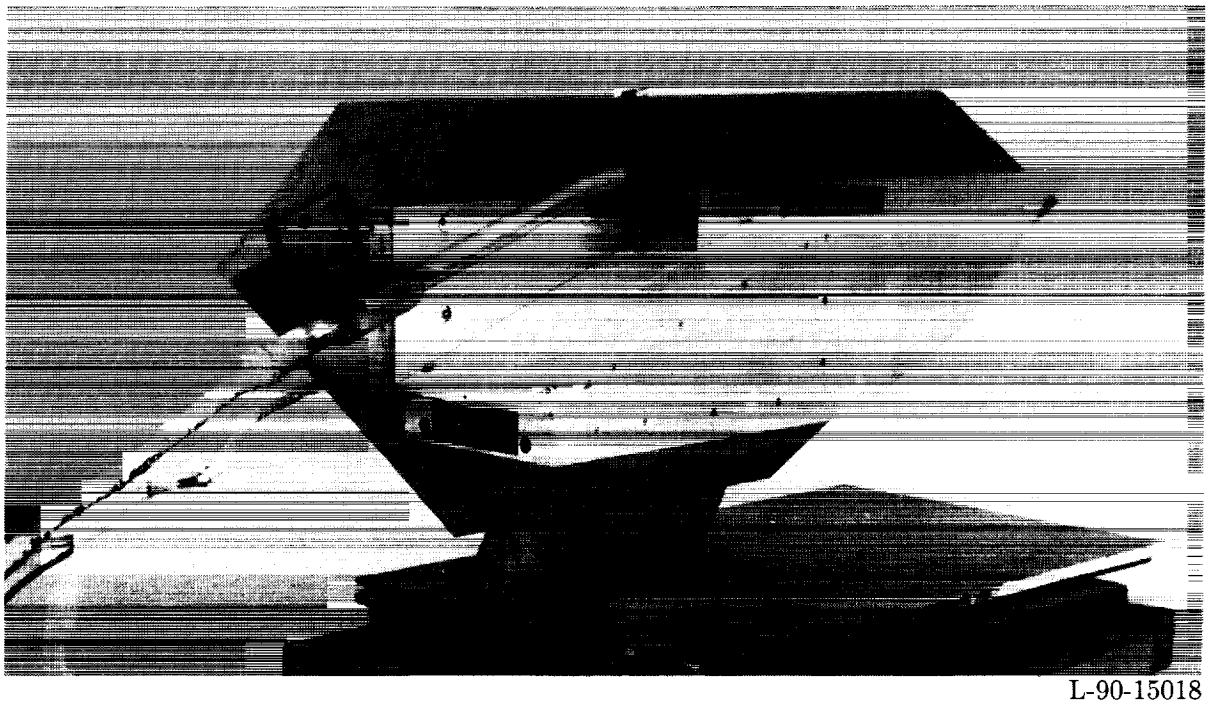

L-90-15018

Figure 3. Photograph of model with rake installed. Uninstrumented expansion-surface-plate configuration.

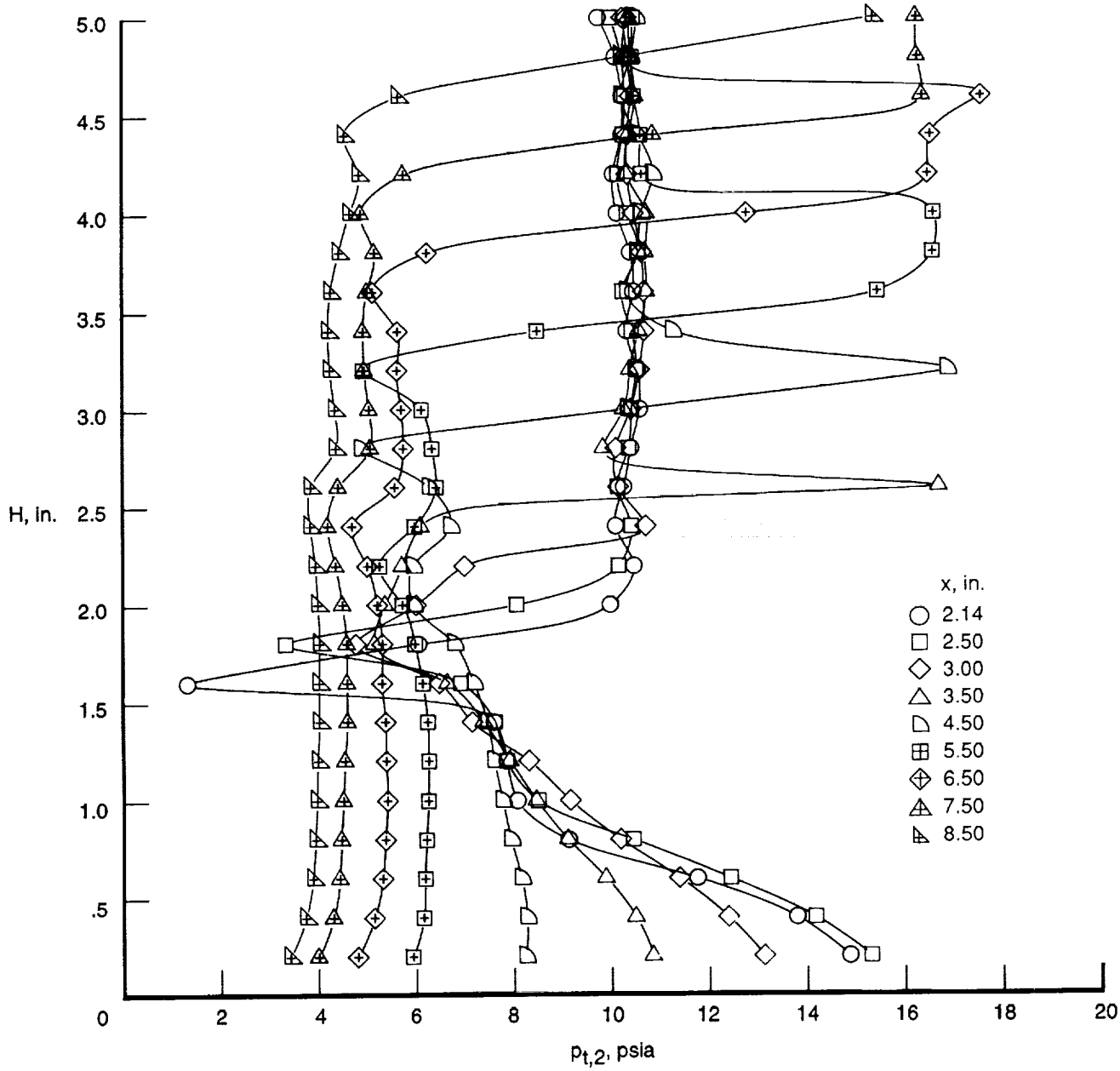

(a) $p_{t,j}$ of ≈28 psia.

Figure 4. Variation of rake pitot pressure with distance from expansion surface for each survey station; flow fence on; simulant gas is Fr-Ar.

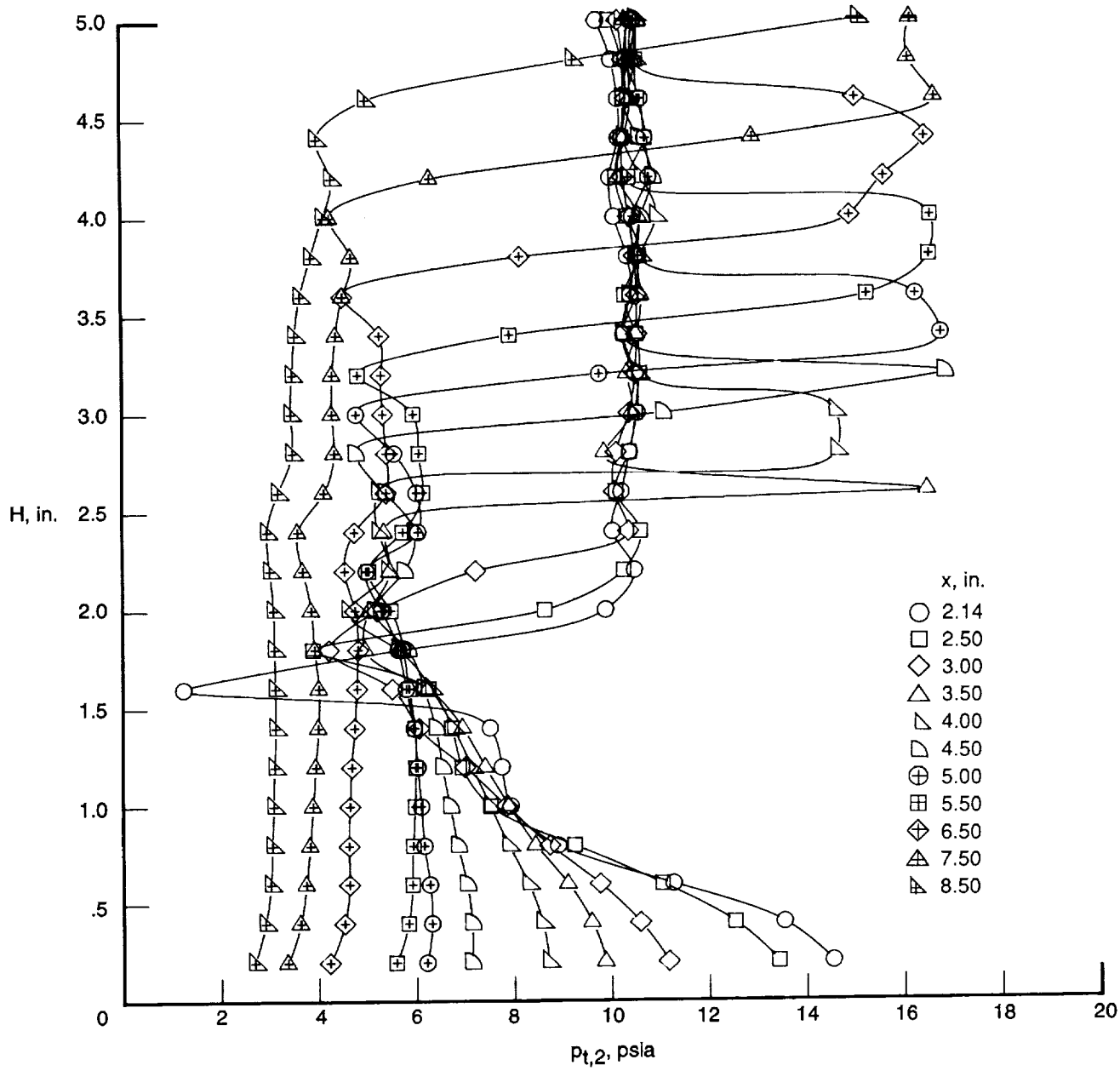

(b) $p_{t,j}$ of ≈14 psia.

Figure 4. Concluded.

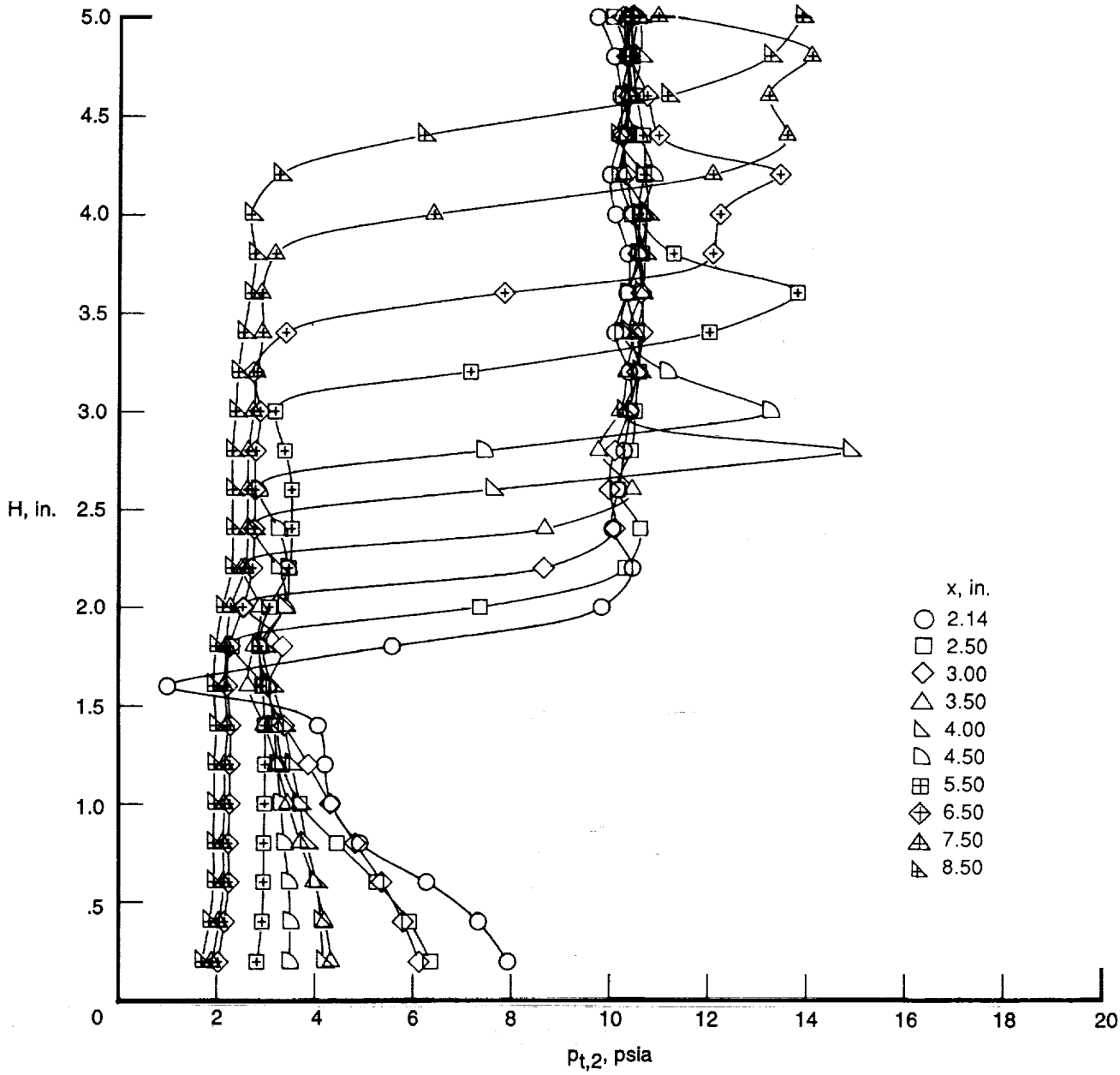

(a) $p_{t,j}$ of ≈28 psia.

Figure 5. Variation of rake pitot pressure with distance from expansion surface for each survey station; flow fence off; simulant gas is Fr-Ar.

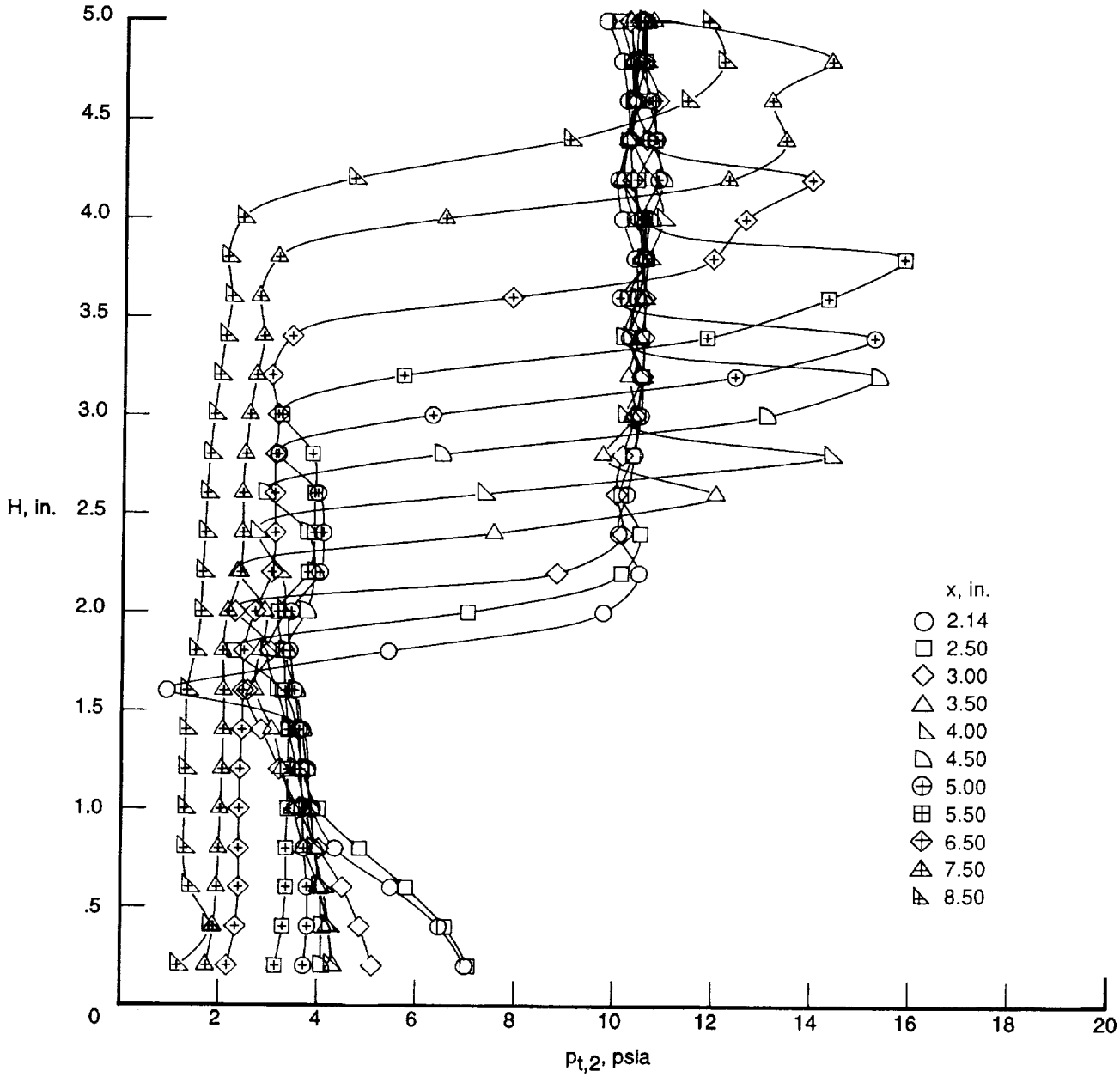

(b) $p_{t,j}$ of ≈14 psia.

Figure 5. Concluded.

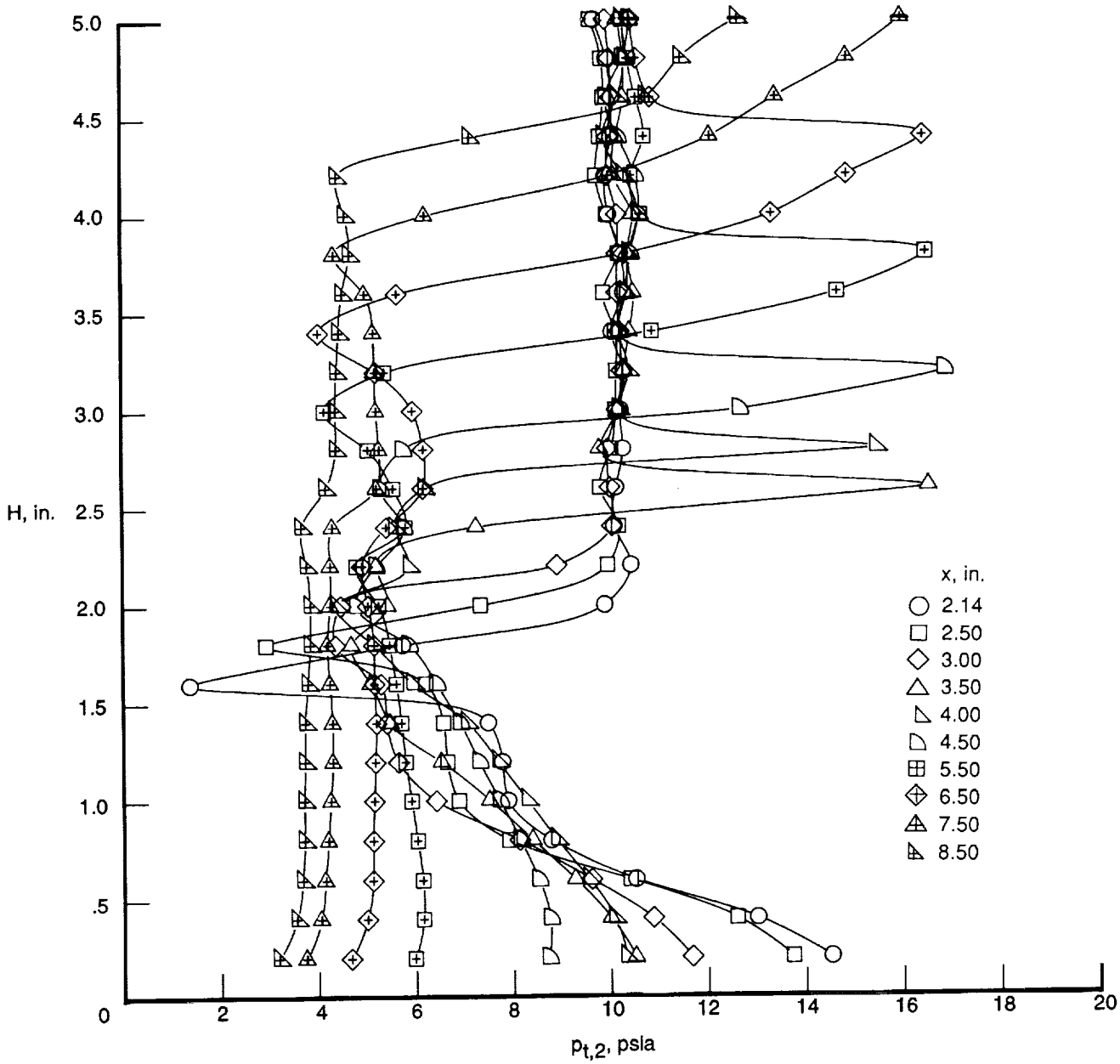

(a) $p_{t,j}$ of ≈28 psia.

Figure 6. Variation of rake pitot pressure with distance from expansion surface for each survey station; flow fence on; simulant gas is air.

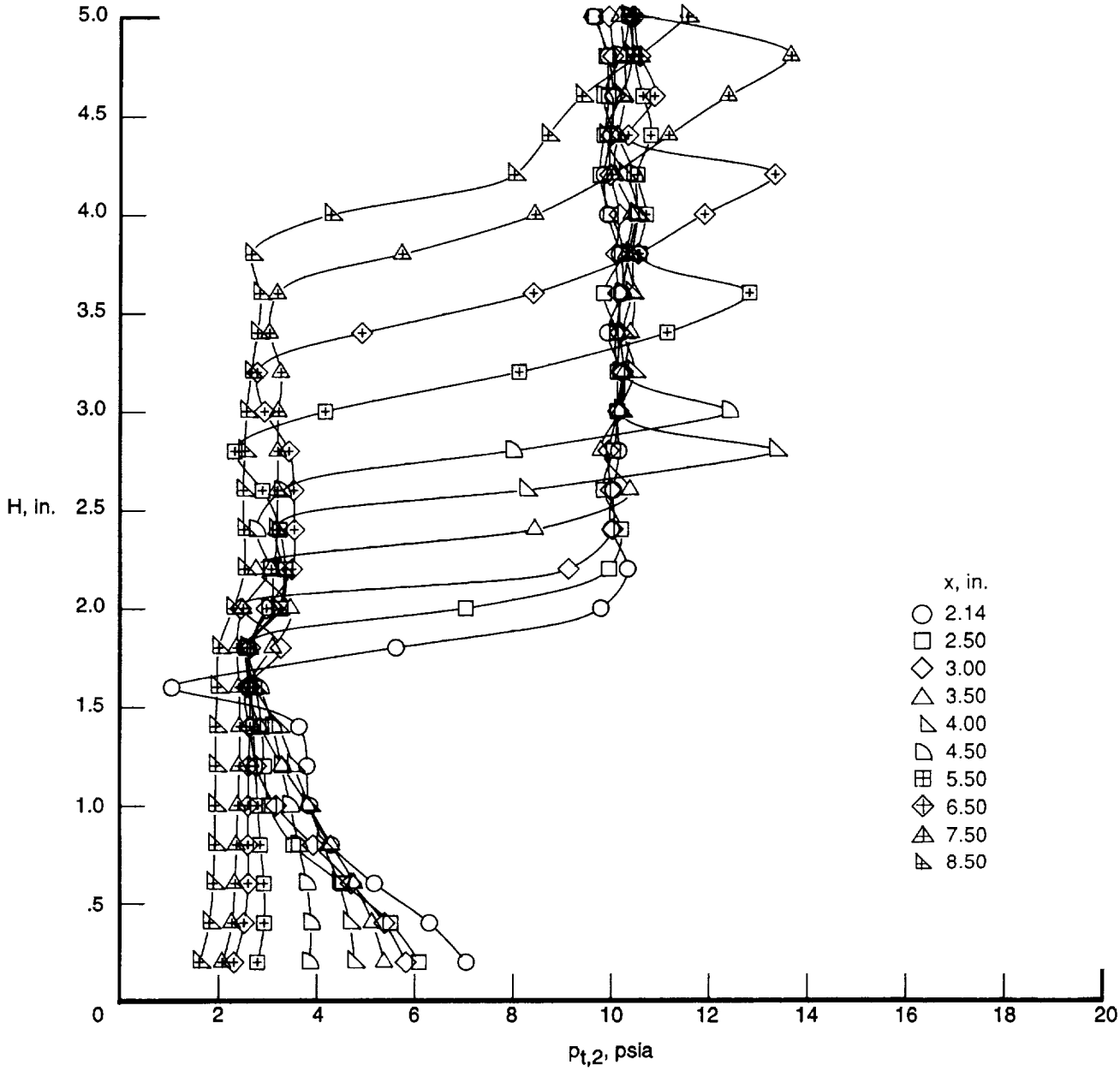

(b) $p_{t,j}$ of ≈14 psia.

Figure 6. Concluded.

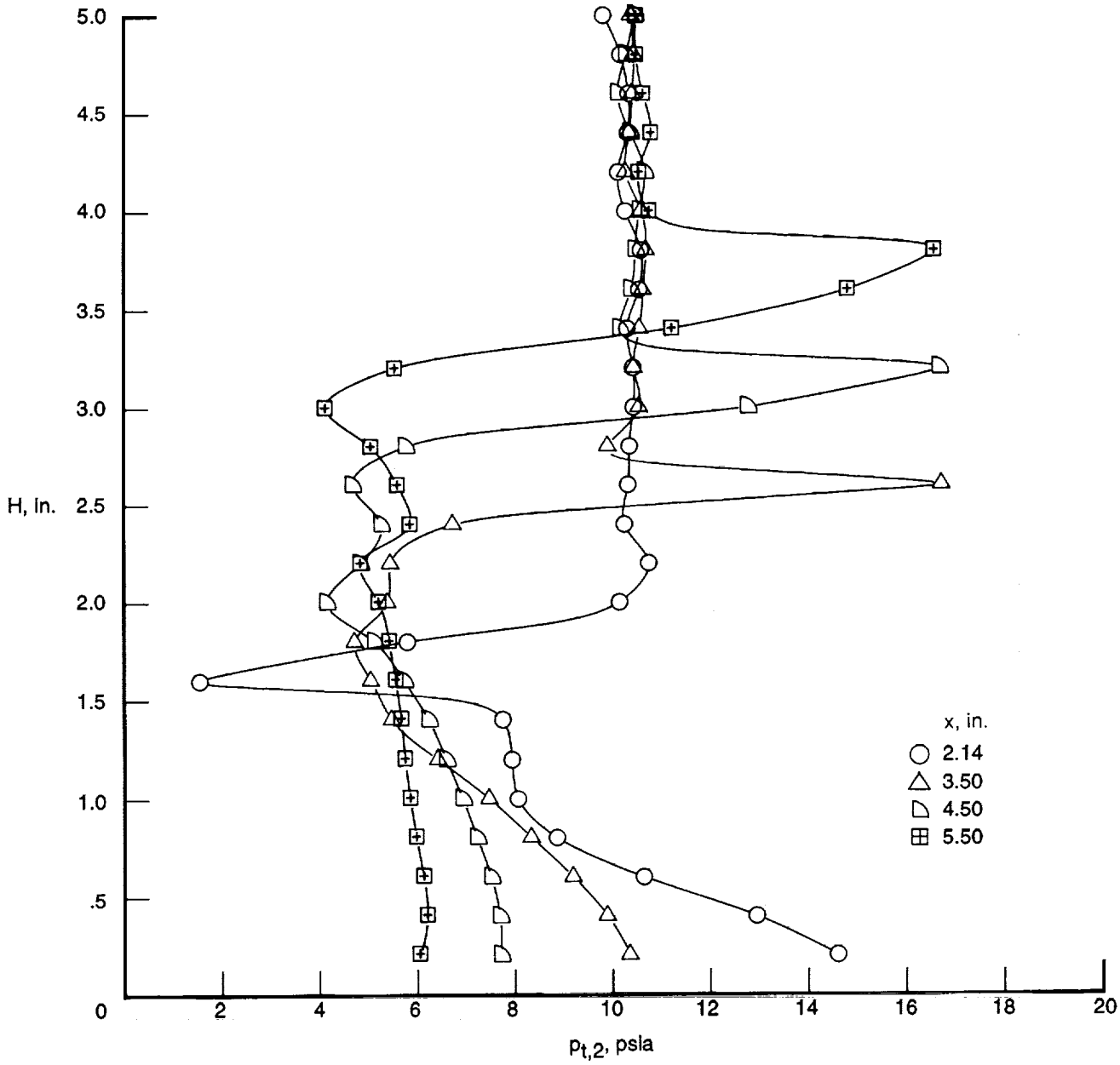

(a) $p_{t,j}$ of ≈28 psia.

Figure 7. Variation of rake pitot pressure with distance from expansion surface for each survey station; flow fence off; simulant gas is air.

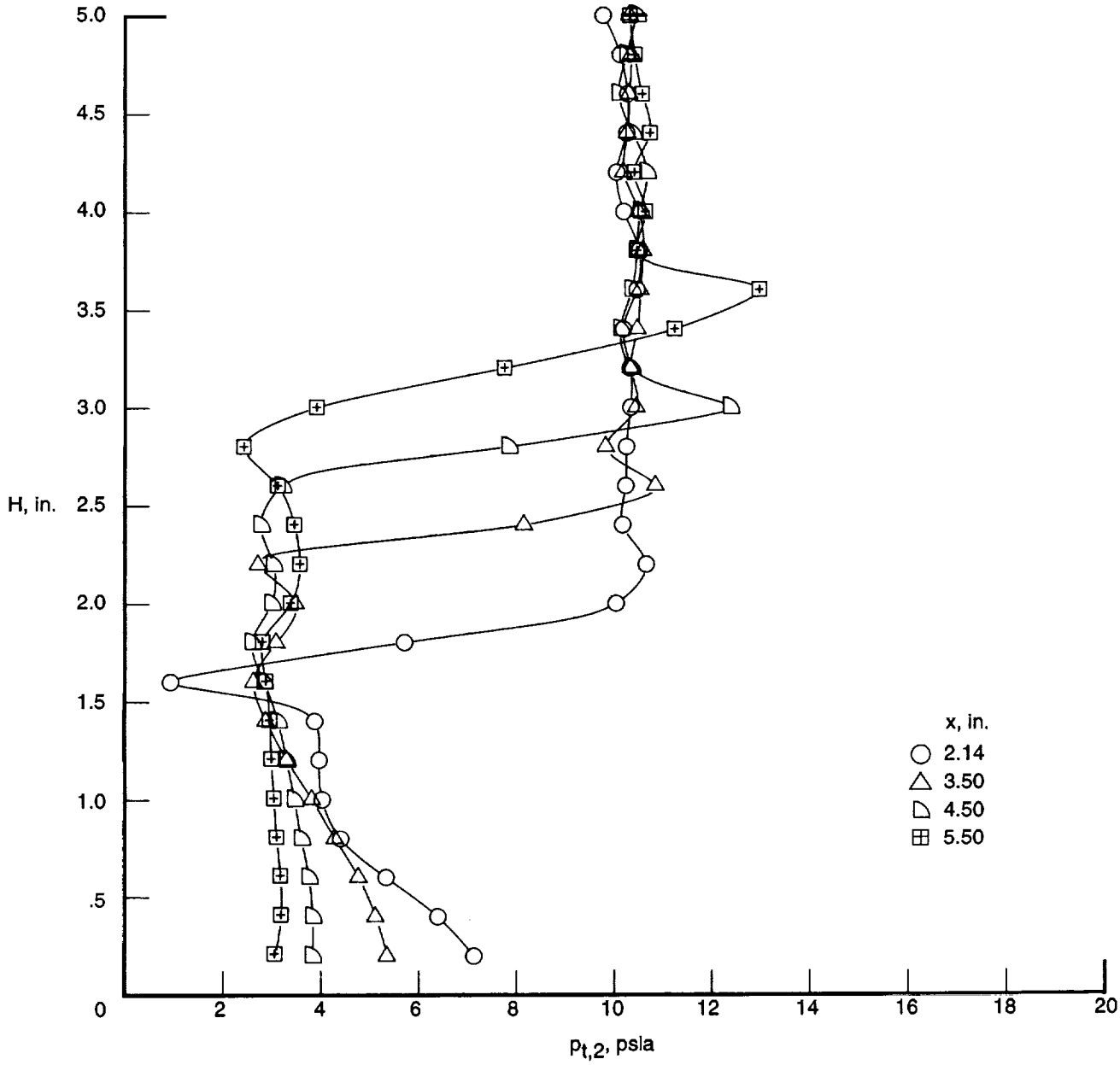

(b) $p_{t,j}$ of ≈14 psia.

Figure 7. Concluded.

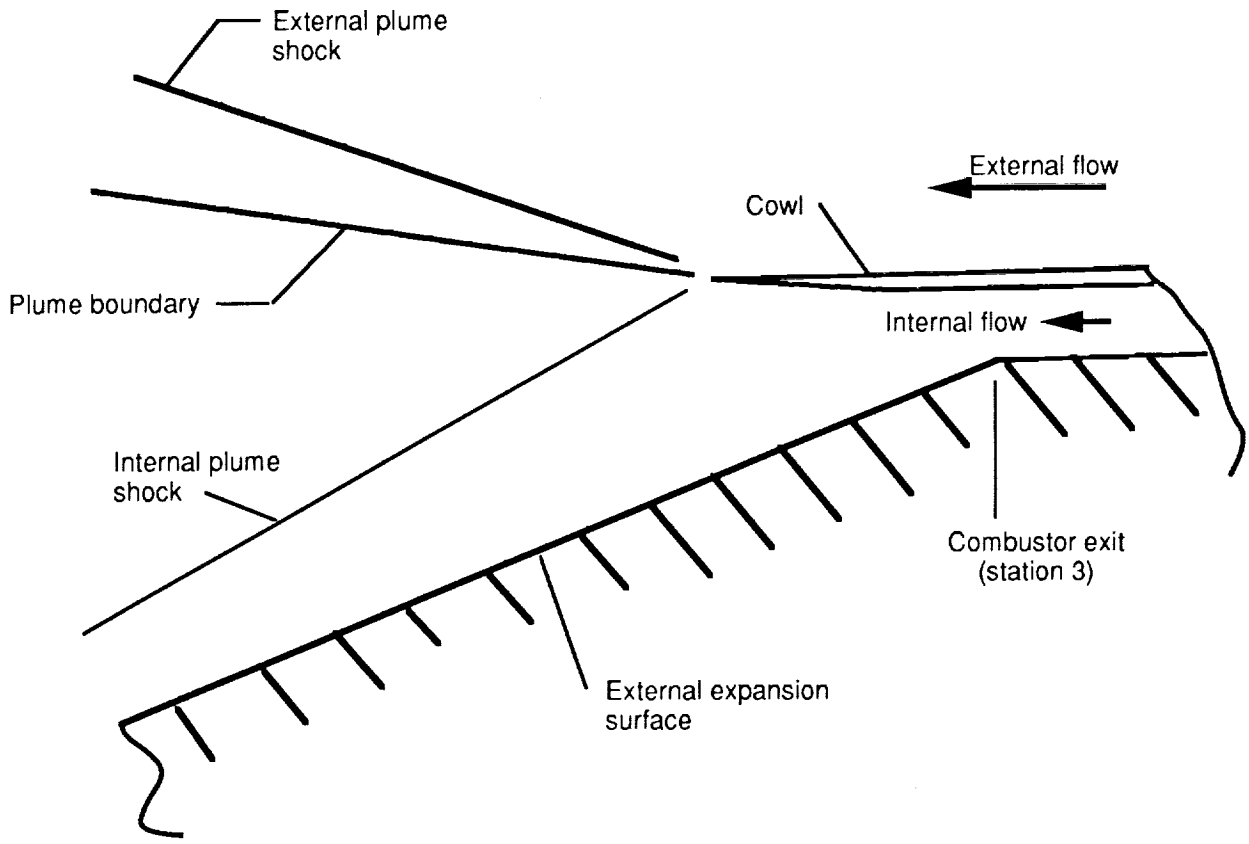

Figure 8. Sketch that illustrates 2-D nozzle exhaust flow.

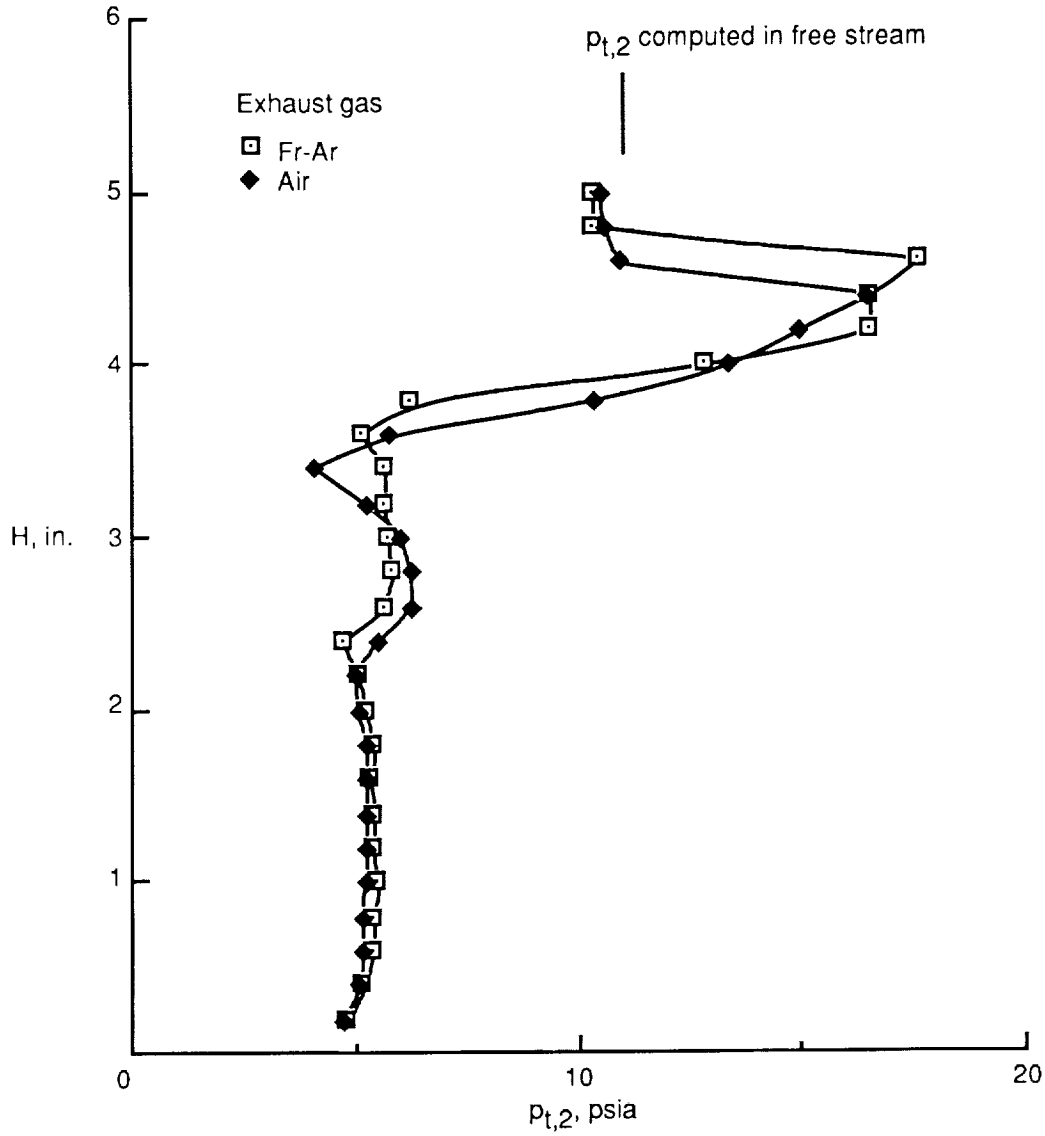

Figure 9. Comparison of pitot profiles for air and Fr-Ar; $x = 6.50$ in.

REPORT DOCUMENTATION PAGE

Form Approved
OMB No. 0704-0188

1. AGENCY USE ONLY *(Leave blank)*	2. REPORT DATE	3. REPORT TYPE AND DATES COVERED
	October 1992	Technical Memorandum

4. TITLE AND SUBTITLE
Pitot Survey of Exhaust Flow Field of a 2-D Scramjet Nozzle at Mach 6 With Air or Freon and Argon Used for Exhaust Simulation

5. FUNDING NUMBERS
WU 505-59-40-03

6. AUTHOR(S)
William J. Monta

7. PERFORMING ORGANIZATION NAME(S) AND ADDRESS(ES)
NASA Langley Research Center
Hampton, VA 23681-0001

8. PERFORMING ORGANIZATION REPORT NUMBER
L-17021

9. SPONSORING/MONITORING AGENCY NAME(S) AND ADDRESS(ES)
National Aeronautics and Space Administration
Washington, DC 20546-0001

10. SPONSORING/MONITORING AGENCY REPORT NUMBER
NASA TM-4361

11. SUPPLEMENTARY NOTES

12a. DISTRIBUTION/AVAILABILITY STATEMENT
Unclassified–Unlimited

Subject Category 02

12b. DISTRIBUTION CODE

13. ABSTRACT *(Maximum 200 words)*

A pitot-rake survey of the simulated exhaust of a half-span scramjet nozzle model was conducted in the Langley 20-Inch Mach 6 Tunnel to provide an additional data set for computational fluid dynamics (CFD) code comparisons. A wind-tunnel model was tested with a 26-tube pitot rake that could be manually positioned along the mid-semispan plane of the model. The model configuration had an external expansion surface of 20° and an internal cowl expansion of 12°; tests were also performed with a flow fence. Tests were conducted at a free-stream Reynolds number of approximately 6.5×10^6 per foot and a model angle of attack of −0.75°. The two exhaust gas mediums that were tested were air and a Freon 12-argon mixture. Each medium was tested at two jet total pressures at approximately 28 and 14 psia. This document presents the flow-field survey results in graphical as well as tabular form, and several observations concerning the results are discussed. The surveys reveal the major expected flow-field characteristics for each test configuration. For a 50-percent Freon 12 and 50-percent argon mixture by volume (Fr-Ar), the exhaust jet pitot pressures were slightly higher than those for air. The addition of a flow fence slightly raised the pitot pressures for the Fr-Ar mixture, but it produced little change for air. For the Fr-Ar exhaust, the plume was larger and the region between the shock wave and plume was smaller.

14. SUBJECT TERMS	15. NUMBER OF PAGES
Flow-field survey; Hypersonic speed; Scramjet exhaust simulation; Nozzle exhaust flow	32
	16. PRICE CODE A03

17. SECURITY CLASSIFICATION OF REPORT	18. SECURITY CLASSIFICATION OF THIS PAGE	19. SECURITY CLASSIFICATION OF ABSTRACT	20. LIMITATION OF ABSTRACT
Unclassified	Unclassified		

NSN 7540-01-280-5500

Standard Form 298(Rev. 2-89)
Prescribed by ANSI Std. Z39-18
298-102

NASA-Langley, 1992